2012

Computational Fluid Dynamics and Heat Transfer Analysis for a Novel Heat Exchanger

Haolin Ma
Lehigh University

Computational Fluid Dynamics and Heat Transfer Analysis for a Novel Heat Exchanger

by

Haolin Ma

A Thesis

Presented to the Graduate and Research Committee

of Lehigh University

in Candidacy for the Degree of

Master of Sciences

in

Mechanical Engineering

Lehigh University

October 17, 2012

Haolin Ma

Thesis is accepted and approved in partial fulfillment of the requirements for the Master of Science in Mechanical Engineering

Computational Fluid Dynamics and Heat Transfer Analysis for a Novel Heat Exchanger

Haolin Ma

_____

Date Approved

_____

Thesis Advisor

_____

(Name of Department Chair)

ACKNOWLEDGEMENT

I would like to express my sincere gratitude and appreciation to everyone who contributed to this thesis. First I'd like to thank my advisor, Dr. Alparsian Oztekin for his extensive guidance and assistance during the past two years. It would have been impossible for me to finish this research without his continuous support and encouragement.

Thank Dr. Sedat Yayla for providing a motivation for this research and the experimental data. I also would like to thank Ali Elmozughi for his suggestions and help learning how to use ANSYS FLUENT. And I'd like to thank all my colleagues and friends at Lehigh University, who provided continuous encouragement and support during my study at Lehigh.

At last, I want give my thank to my parents, Mr. Jianwei Ma and Mrs. Dongying Ma and my fiancé, Ms. Tingting Li, for their tireless support.

Table of Content

ACKNOWLEDGEMENT iv

Table of Content v

List of Figures vii

List of Tables ix

Abstract 1

Chapter 1.Introduction 2

Chapter 2.Computational Domain and Mesh Generation 7

2.1 Experimental test section 7

2.2 Computational Domain 8

2.3 Meshing and Spectral Convergence 10

Chapter 3.Mathematical Model and Numerical Methods 15

3.1 Boundary conditions 15

3.2 Turbulent Flow Model 16

3.3 k-ε RANS Model 20

3.4 Heat Transfer Model 22

3.5 Solution Procedure 23

Chapter 4. Results Discussion 24

4.1 Flow Characteristics 24

4.2 Comparison between Simulations & Experiments 30

4.3 Heat Transfer Analysis 37

Chapter 5. Conclusion 43

Reference 45

Vita 48

List of Figures

Figure 1 Schematic of test section of slotted shell-tube heat exchanger 8

Figure2 3D computational domain 9

Figure 3 3D computational domain near the tube bank region 10

Figure 4 Mesh structure of the computational domain 11

Figure 5 Mesh structure (a) near the tube bank, (b) at the interface and (c) in the exit region. The mesh includes 4-million-elements. 12

Figure 6 Velocity profile in the y-direction at x = 437.6 mm and z = 10 mm for Re=1500 using three different mesh levels 14

Figure 7 Residuals in various flow parameters for Re = 700 for a laminar and turbulent flow modeling 18

Figure 8 Stream function for Re =1500 at various cross-sections: (a) z = 8 mm; (b) z = 1 mm; (c) z = 10 mm 26

Figure 9 Vorticity Contours for Re = 1500 at various cross-sections: (a) z = 8 mm; (b) z = 1 mm; (c) z = 10 mm 27

Figure 10 (a) Streamline; (b) Vorticity; (c) Stream-wise velocity; (d) Span-wise velocity; (e) Turbulent kinetic energy contours predicted by 2-D model for Re =1500 28

Figure 11 (a) Streamline; (b) Vorticity; (c) Stream-wise velocity; (d) Span-wise velocity; (e) Turbulent kinetic energy contours predicted by 2-D model for Re = 4000 29

Figure 12 Stream function for Re =1500 predicted by (a) 2D simulation, (b) 3D simulation and (c) observed by experiments 32

Figure 13 Stream function for Re = 4000 predicted by (a) 2D simulation, (b) 3D simulation and (c) observed by experiments **33**

Figure 14 Vorticity contours for Re = 1500 predicted by (a) 2D simulation, (b) 3D simulation and (c) observed by experiments. Minimum value of vorticity is ±1s-1 and the increments is $\Delta\omega$=2s-1 ..... **34**

Figure 15 Vorticity contours for Re = 4000 predicted by (a) 2D simulation, (b) 3D simulation and (c) observed by experiments. Minimum value of vorticity is ±1s-1 and the increments is $\Delta\omega$=2s-1 ..... **35**

Figure 16 Normalized stream-wise velocity [<u>/U], span-wise velocity [<v>/U] and turbulent kinetic energy for Re =4000. Contours at the left column denote results predicted by 3D simulations; contours at the right column denote results obtained by experimental measurements. Minimum of [<u>/U] is 0.025and the minimum of [<v>/U] is 0.05 with the increments of Δ[<u>/U] is 0.025 and the increments of Δ[<v>/U] is 0.05

..... **36**

Figure 17 Isotherms (first row- a, b), streamlines (the second row- c, d) and vorticity field(third row- e, f) for Re =1500 in the wake a tube. Contours at the left column denote results obtained for the non-slotted tube design and the contours at the right denote results for the slotted tube design **39**

Figure 18 Isotherms (first row- a, b), streamlines (the second row- c, d) and vorticity field (third row- e, f) for Re = 4000 in the wake a tube. Contours at the left column denote results obtained for the non-slotted tube design and the contours at the right denote results for the slotted tube design **40**

List of Tables

Table 1 Number of elements in three different levels of mesh. 13

Table 2 Boundary conditions for CFD and heat transfer simulations 16

Table 3 The list of Reynolds number simulations conducted at various flow rates 17

Table 4 Averaged heat transfer coefficient for non-slot design 38

Table 5 Comparison of heat transfer performance between slotted and non-slotted heat exchanger designs for Re = 700, 1500, 4000 and 6000 42

Abstract

Computational fluid dynamics and heat transfer simulations are conducted for a novel shell-tube type heat exchanger. The heat exchanger consists of tube with a narrow slot oriented in the stream-wise direction. Numerical simulations are conducted for the Reynolds number from 700 to 6000. The 3D turbulent flow in the tube bank region is modeled by k-ε Reynolds stress averaging method by employing ANSYS FLUENT. 3-D and 2-D transient flow and heat transfer simulations are compared to determine the effects of wall on the flow structure. The wall influence the spatial structure of the vortices formed in the wake of tubes and near the exit of slots. The flow structure predicted and observed is compared. The agreement between the predicted 3-D flow structure and PIV flow visualization results verifies the numerical method and the turbulent model employed here. The slotted tube heat exchanger improved heat transfer by more than 50% compare to the traditional shell-tube heat exchanger without slots.

Chapter 1.Introduction

Due to the high consumption and the reducing availability of fossil fuel resource, high thermal performance heat exchanger is subject to great interest over decades. Typically, two fluids with different temperature circulate through the heat exchanger in natural or forced convection manners and the thermal energy is exchanged via surfaces during the process. There are two primary flow arrangements in the heat exchanger: a parallel-flow and a counter-flow. Two fluids travel from the same end to another end in the parallel-flow heat exchanger. For the counter-flow arrangement, the two fluids run in the opposite direction from two ends of the heat exchanger. The arrangement for the flow direction leads to the efficiency difference. The counter-flow path provide higher heat transfer, benefiting from the more uniform temperature difference and relatively high flow rate, compared to the parallel-flow path. To improve the efficiency of the heat exchanger, maximizing the surface area of the wall between two fluids and minimizing resistance flow passing across the exchanger are two most concerned focuses. Different approaches have been made on these two directions. The increase of area is the most direct way to exchange more thermal energy. However, the efficiency and the performance do not increase, following the area increment, alongside the area increase results in a higher expense of manufacturing. Additionally, the working space requirement is another limiting factor. Another direction is the faster fluid transportation in heat exchanger to make the rate of thermal exchange to be higher. Flow resistance can be reduced by a higher surface finish or by adding nanoparticles and polymer additives [1]. The increased cost of manufacturing and the stability of additives and the erosion of the facilities due to

added particles constrained the development. Improving the efficiency and the performance of is an important topic of research.

Based on the construction, heat exchangers can be classified as plate and shell & tube types. In plate heat exchanger (PHE), fluids, spreading over the plates, are exposed to a broad surface area, which largely increases the heat transfer. For a compact or a size-sensitive heat exchanger, PHE can provide relatively high efficiency by maximizing the surface area in a limited space. Experimental studies on a PHE with different chevron plate arrangements were performed. It has been shown that the Nusselt number were increased by five folds [2]. A shell and tube heat exchanger is the most widely used. The heat transfer can significantly be enhanced by flow mixing and turbulence. Typically, the first row of tubes is served as turbulent actuator and the turbulence can help improve the heat transfer through the tube bank. Auxiliary objects near or attached to the tubes can increase the turbulence as well. Leu et al. found that block shape vortex generators mounted at a span angle of 45°behind the tubes provided the best heat transfer augmentation [3]. Winglet-type vortex generators, being placed with a heretofore-unused orientation, improved the heat transfer in staggered tube banks by 30% to 10% for Reynolds number from 350 to 2100 [4]. Further exploration for delta winglet vortex generators by Seong Won Hwang showed that the efficiency depended on the size and the shape of delta winglet, the location where it is implemented [5]. Tube arrangement also influences the efficiency and the performance of the shell-tube heat exchangers. Jinin-Yuh Jang and Li-Kwen Chen presented a wavy-fin design and stated that the increased waviness angle and the decreased waviness height lead to a higher Nusselt number [6]. Nuntaphan et al. proposed correlations to predict heat transfer of heat exchangers using

crimped spiral fins. They show that a good predictive ability against the test data [7]. Elliptic tubes were investigated and compared with conventional circular ones for heat transfer. It has been reported that elliptic tubes enhance heat transfer by 13% [8]. Investigations for flow inside of the tube have also been performed. Smith et al. presented the experimental results for tubes fitted with helical screw tape and stated that the increase of average Nusselt number was 230% and 340%, respectively for with and without core-rod inserted, compared to conventional plain tube [9].Further experiments on the twisted tape, inserted into the tube, in clockwise and counterclockwise had been carried out with the different twist ration and angles [10]. Segmental baffles in heat exchanger can guide the flow across the tube bundle and prevent the tubes from vibrating and sagging. 3D simulations on the middle-overlapped helical baffles were carried out with different helical angles [11].

Investigations and improvements working on the traditional circular tube bank have been found in many different numerical methods and computational fluid dynamic (CFD) codes, both in laminar and turbulent regime. Numerical analysis by an integral method of boundary layer was used to investigate the heat transfer for the tube bank [12]. And an entropy generation minimization method is used to optimize the geometric parameters in design of tube bank [13]. Design optimizations of heat exchangers were found in size of tubes with the spacing and arrangements by different algorithms [14-18]. Analysis of laminar flow across the tube bank in in-line [19] and staggered [20] manners were performed and showed good agreements with present experiments and empirical correlations. Turbulent flow simulation for staggered tube bank was also carried out with Reynolds stress analyzing method by You Qing Wang [21]. In the downstream of flow

passing across a tube bank, a horseshoe vortex is captured by numerical simulations and studied on its influence of the vortex-excited vibration to the tube [22,23].

The horseshoe vortex phenomena have been studied by experiments long before. Experiments with pertinent data for flow pass tube bank either in in-line or staggered manners have been performed date back to 1933.Review on periodic phenomena for flow passing cylinders was done by Berger and Willey [24] and Williamson brought up new understandings, also new questions, on this topic, with the help of PIV(Particle-Image-Velocimetry) and direct numerical simulations [25]. Relationship between the vortex shedding lock-on behavior and the heat transfer was established by experiment [26].

Extensive experiments were carried out for helping design cross flow heat exchangers. Colburn proposed a simple correlation for heat transfer of flow passing across tube bank [27]. Zukauskas [28,29] and Ulinskas [29] presented future experimental data for heat transfer in a tube bank in a cross flow, which provided more detailed correlations. The correlations work well for 10 or more tubes in staggered configuration and for $10<Re<40{,}000$. A tabulated data for correlations, which made the correlations to be easy to use, was presented by Incropera [30].

Dating back to 1993, slit across the tube is first introduced into the heat exchanger design by Popiel et al. in the study of the vortex shedding for flow passing circular tube bundle with rear concave surface [31]. The slit increased the surface area and induced strong vortices, however vertical slit is not the best way to improve the heat transfer and could only bring smaller temperature difference between the two fluids, running in the heat exchanger. Yayla first considered a horizontal stream-wise slot and he documented a PIV flow visualization for flow passing an arrays of slotted cylinders. The experimental

results indicate that the intensity of turbulence is increased in a tube bank. The present work will investigate the effect of the slotted tube on the performance of the heat transfer.

This thesis is organized in the following manner. The diagram of an innovative design, slotted tube bank heat exchanger, and CFD computational domain are presented in Chapter two. The mathematical model and the detailed numerical method are described in Chapter three. The results are presented and discussed in Chapter four. Conclusions are given in Chapter five.

Chapter 2.Computational Domain and Mesh Generation

Commercial CFD codes have been developed and improved for decades. ANSYS provides a system level modeling, meshing and complex flow simulations. The 3D geometry generated by "Solidworks" is modified by using “Design Modular” into two computational zones for an adaptive meshing. The equations governing the velocity and temperature fields are discretized using two zone mesh and the resulting equations are solved using an iteration method, ANSYS FLUENT. “CFD-Post” and “Tecplot” are used to present the results of simulations in a graphical form.

2.1 Experimental test section

Yayla has conducted Particle Image Velocimetry experiments for flow passing slotted-tube-bank [32]. The experiments were done in a water channel with a test section of 0.4 m in depth, 1 m in length and 0.02 m in width, as shown in Figure1. The dimensions of the slotted tube bank are characterized by S_D, S_T and S_L, diagonal pitch, span-wise pitch and longitudinal pitch between two consecutive tubes, respectively.

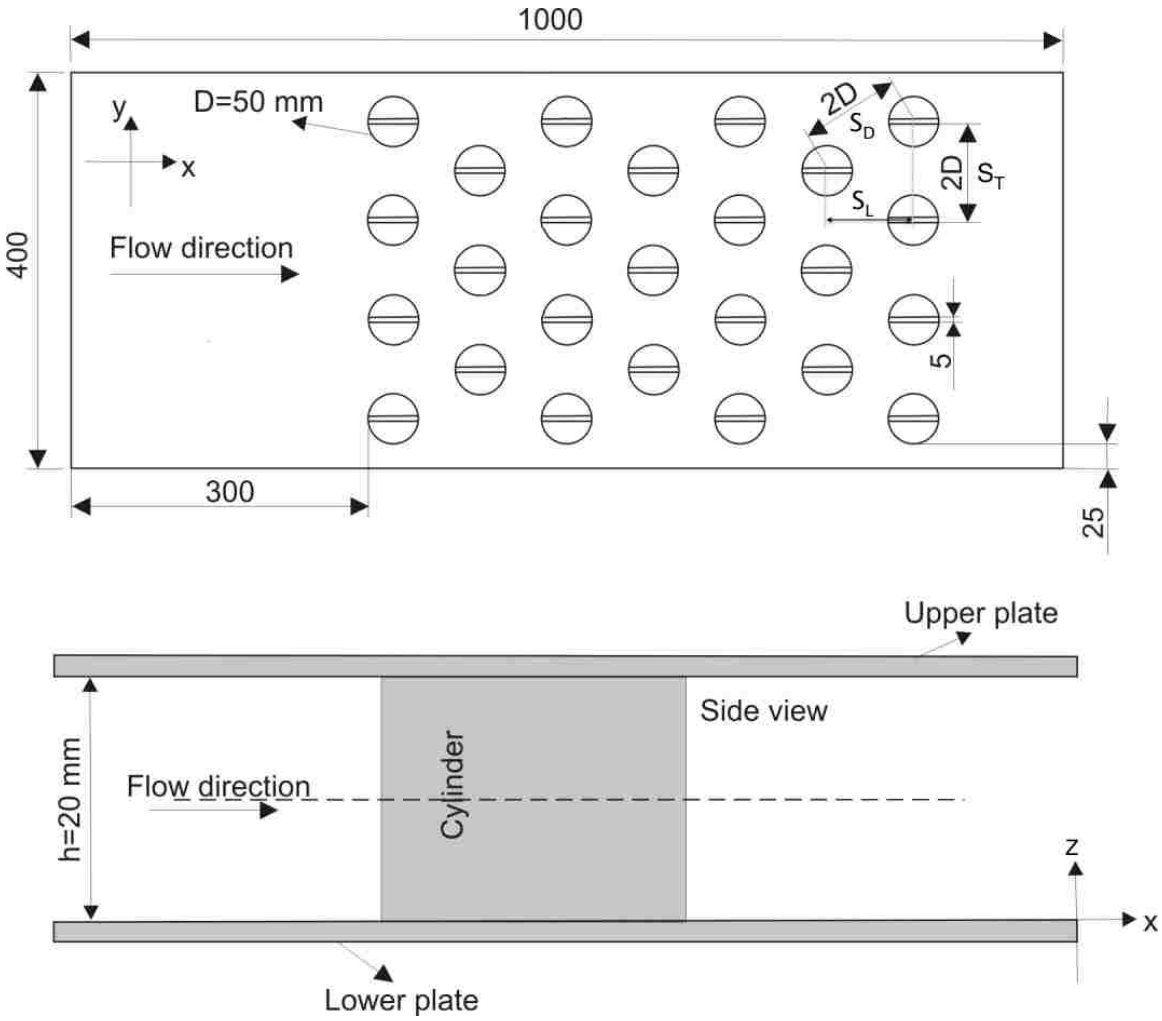

Figure 1 Schematic of test section of slotted shell-tube heat exchanger

2.2 Computational Domain

Numerical simulations are conducted in a computational domain that has the same dimensions of the bank tube as in the experiment. Fully developed velocity profile is considered at the inlet. The length of the channel between the inlet and the tube bank zone is 6D. It does not have to be long since the velocity profile at the inlet is set to be fully developed. More detailed discussions for the inlet condition are presented in *3.1*.

The flow structure in the tube bank can be influenced by the conditions imposed on the velocity field at the inlet and the outlet. To minimize such influence on the flow

characteristics, a long exit region is considered, which will lead to the fully developed flow away from the tube bank region. The 3D computational domain for the simulation is illustrated in Figure 2 and the 3D computational domain for the tube bank region is shown in Figure3.

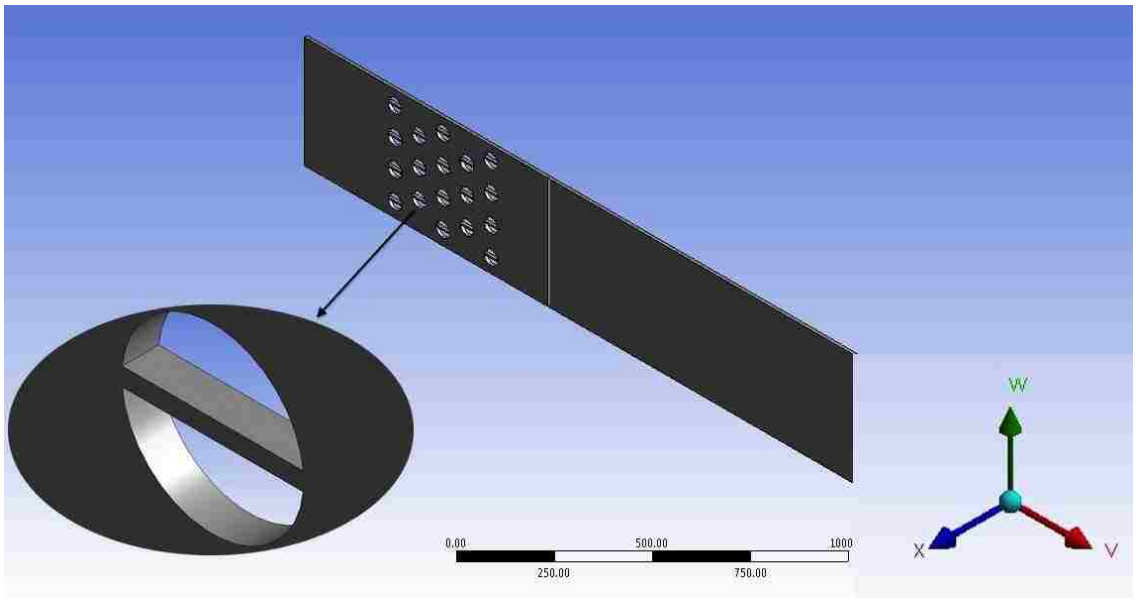

Figure2 3D computational domain

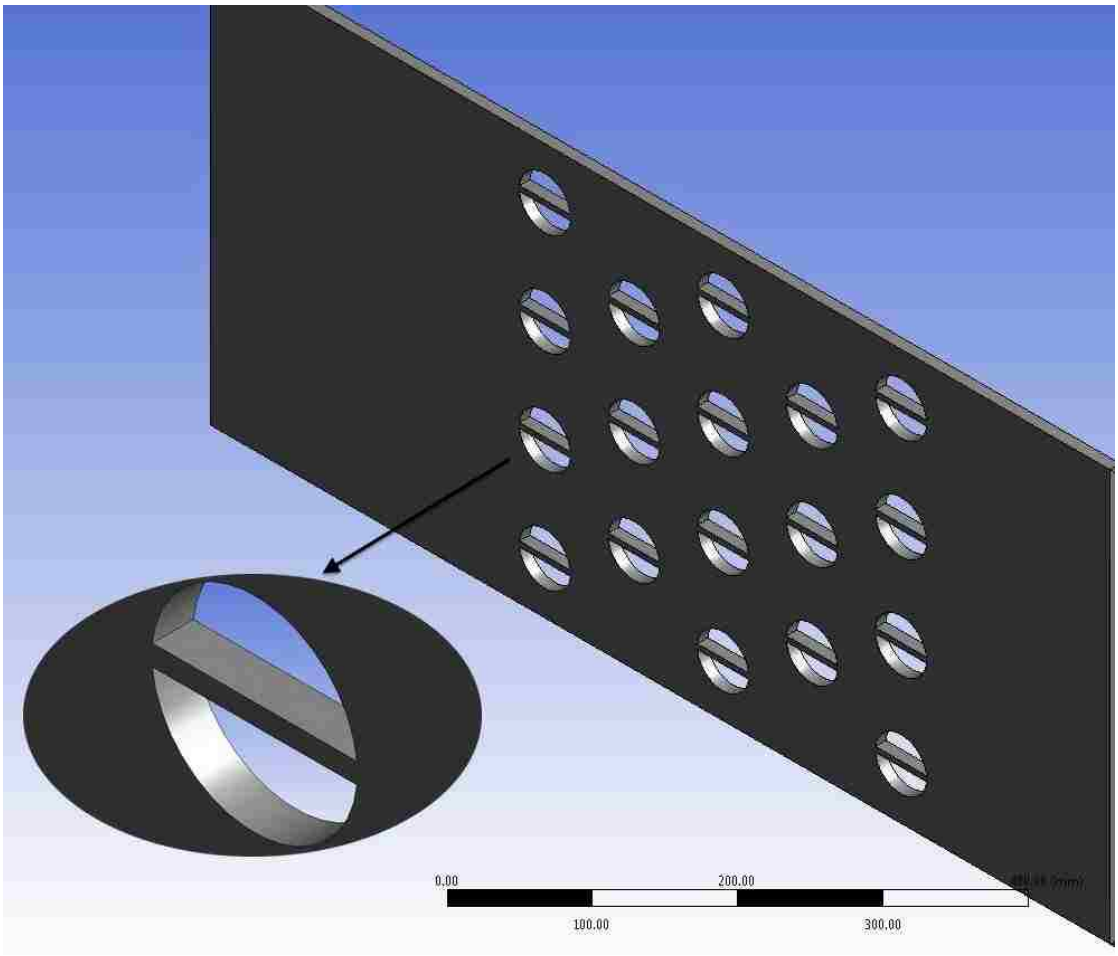

Figure 3 3D computational domain near the tube bank region

2.3 Meshing and Spectral Convergence

A high quality mesh is very important for successful numerical simulations. The smaller the size of the element near the wall of the tube and the slot, the more detailed and accurate flow structure will be captured. However, for the 3D simulation, a small change in the size of element will lead a substantial increase in the number of elements. That will results in a significant increase of computational time. In order to balance the accuracy of the simulations and CPU time, an optimum size of mesh need to be chosen.

Due to the symmetry of the flow domain in y and z axis, the simulations are conducted for the 1/4 of the computational domain by symmetry plane. “Symmetry”

boundary condition is imposed on the velocity field at y = 0 mm and z = 0 mm. The computational domain is divided into two zones: the inlet and tube bank zone and the exit zone. Data are transferred between the two zones by the connective interface. Non-uniform meshing is used to discretize the equations in the inlet and tube bank zone. An inflation method is applied at the wall of tubes. The boundary layers on walls of tubes, upper and lower bounds are refined by putting several inflation layers. A coarser non-uniform mesh is employed in the exit region. At the interface between the two zones, contact sizing is applied for coordinating the finer mesh in the inlet and tube bank zone and the coarser mesh in the exit zone.Figure4 depicts how the coarse and fine mesh is distributed in the computational domain.

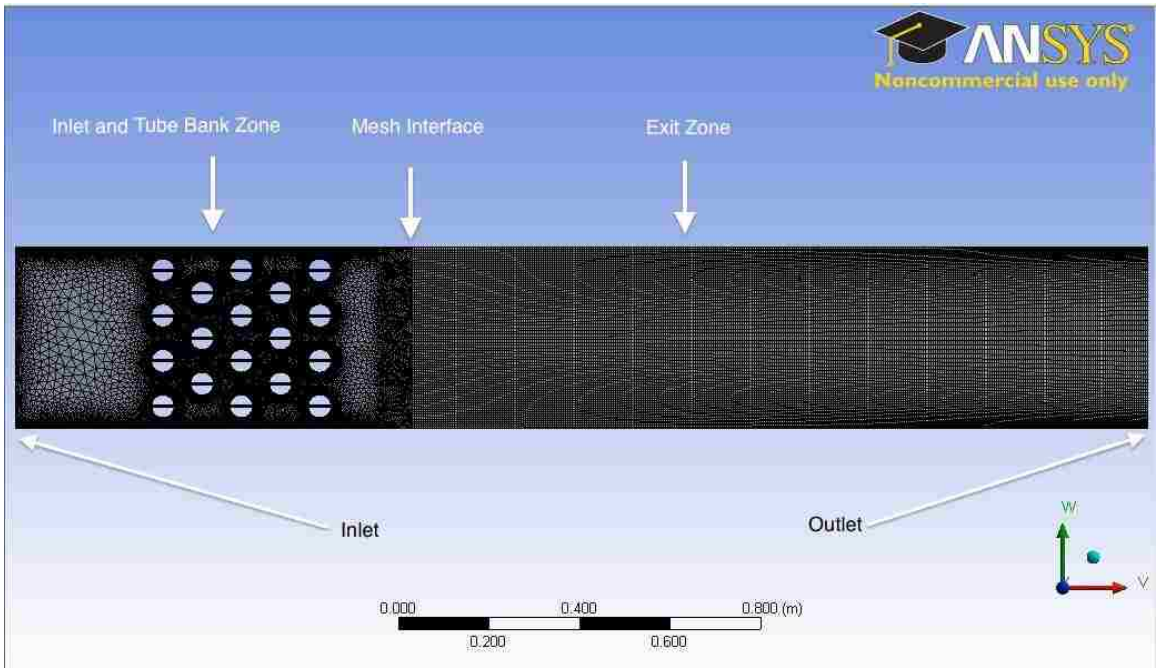

Figure 4 Mesh structure of the computational domain

By adjusting the global size of mesh element, contact size at the interface and inflation layers near the wall of the tubes, three meshes with different magnitudes of elements in the tube bank zone are generated. These three different levels of meshing are

referred as “Coarse”, “Fine” and “Finer” mesh. The spectral convergence test and computational performance are performed on the three meshes. The mesh structure near the tube bank region, at the interface and in the exit region is displayed in Figure 5. The mesh near the wall of the tubes and near the slots is dense, as shown in Figure5a.

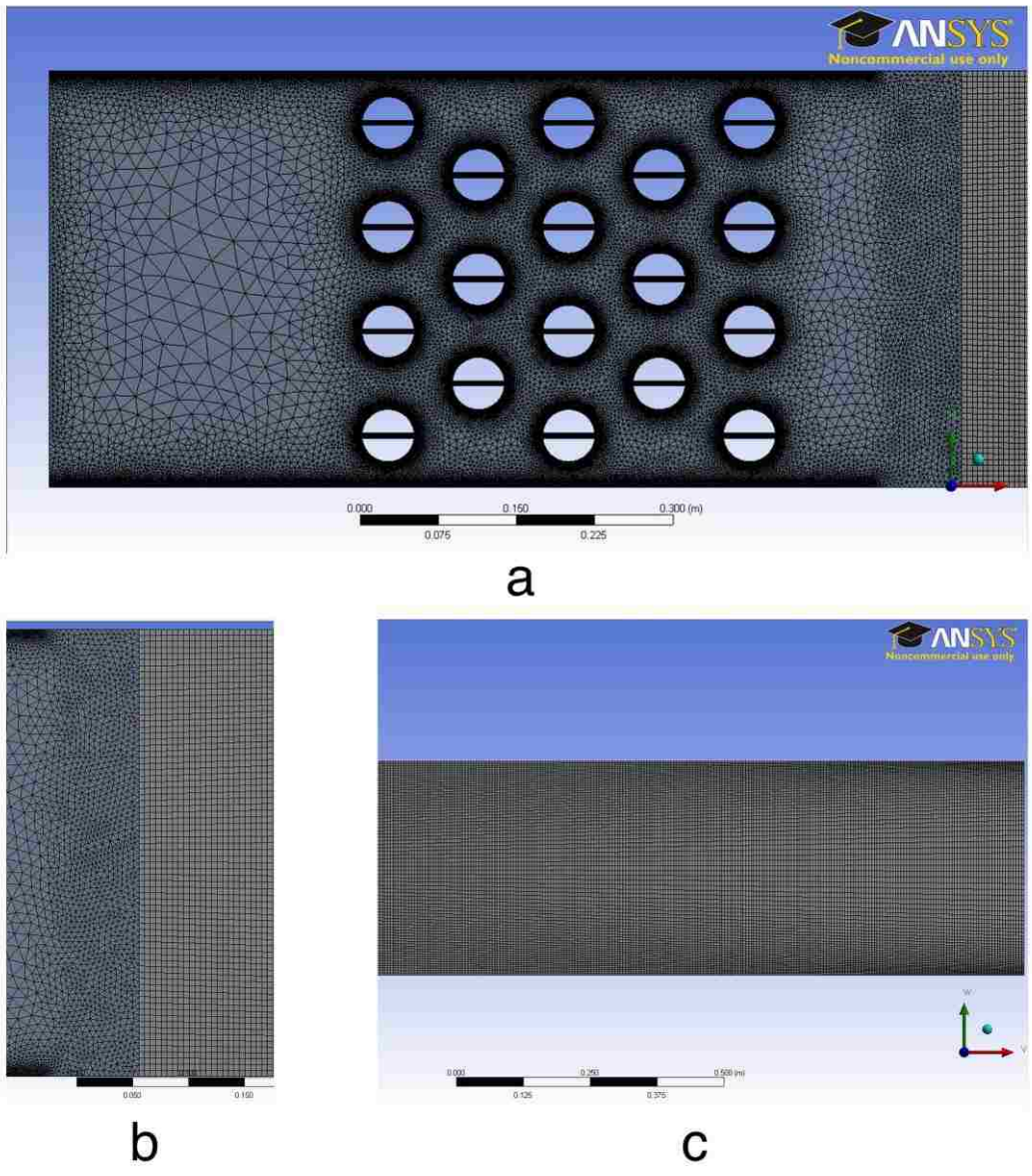

Figure 5 Mesh structure (a) near the tube bank, (b) at the interface and (c) in the exit region. The mesh includes 4-million-elements.

The total number of mesh in the computational domain and in these tube zones are listed in Table 1 for a “Coarse”, a “Fine” and a “Finer” level mesh. The number of elements near the tube bank region is calculated in FLUENT for each mesh. Number of elements for the “Finer” mesh doubles compared to that for the “Coarse” mesh. Number of elements in the tube region can be increased significantly with a slight increase of element in the inlet and the outlet region. With the use of two zone meshing, the mesh in the tube zone can be refined with a minimal increase of CPU time. That enables us to obtain very accurate 3-D flow structure in the tube zone.

Mesh	Num. of elements near tubes	Num. of elements in total domain
Coarse	1,795,299	2 million
Fine	2,388,150	3 million
Finer	3,613,676	4 million

Table 1 Number of elements in three different levels of mesh.

The velocity profile, in the y-direction at x= 437.6 mm and z=10 mm, is plotted in Figure6 for different level of mesh. The velocity profile differs slightly at the center and near the walls as the mesh level is altered. The velocity profiles obtained using a “Fine” mesh and a “Finer” mesh are nearly the same with a slight variation near the walls, as seen in Figure6. This concluded that the fine mesh is sufficient to satisfy the spectral convergence. Fine mesh is used to perform the simulations to obtain the results presented in the next chapter for various flow conditions.

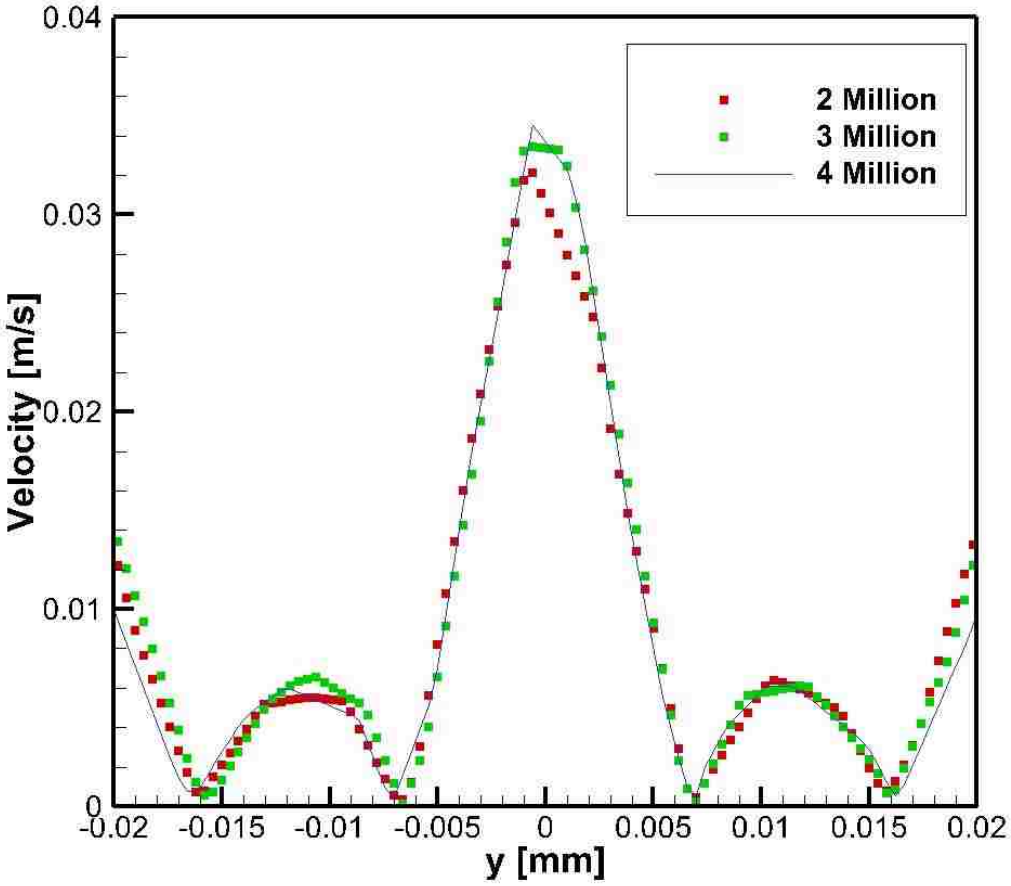

Figure 6 Velocity profile in the y-direction at x = 437.6 mm and z = 10 mm for Re=1500 using three different mesh levels

Chapter 3.Mathematical Model and Numerical Methods

The equations governing the incompressible fluid motion and the heat transfer from tubes to the flow with fluid passing tubes are presented in this Chapter. Boundary conditions imposed on the velocity field at the inlet, outlet, the tube surfaces and the wall of channel are described. The thermal boundary conditions are also described in this Chapter.

3.1 Boundary conditions

In order to simulate the conditions observed in the experiments, the fully developed parabolic velocity profile needs to be obtained before the fluid enter the tube bundles. The parabolic velocity profile in a laminar flow and the empirical power-law equation in a turbulent flow in the channel with a circular cross-section is obtained and verified [33]. For flow in a channel with a rectangular cross-section, there has been no equation or correlations for describing the fully developed velocity profile. To make the inlet velocity profile to be similar as in the experiment, the flow simulation is performed in a straight channel without the tube bundles. At the outlet of the straight duct, the velocity profile is acquired. As Reynolds number is changed, the length of the channel needed to obtain the fully developed velocity profile is adjusted. The generated velocity profile at the exit of the straight channel is imported into FLUENT and is used as the inlet velocity profile for the simulation in the channel, including the tube bundles.

The full set of boundary conditions imposed on the flow field and the thermal boundary conditions imposed on the temperature field are listed in *Table 2*.

	Flow Simulation	Heat Transfer Simulation
Inlet	Fully developed velocity profile	Uniform temperature at 293 K
Outlet	Zero Pressure Outlet	$\frac{\partial T}{\partial x} = 0$
Wall of the Tube	Standard no slip wall on no penetration	Constant temperature at 393K
Wall of the Duct	Standard no slip wall on no penetration	Adiabatic wall
Symmetry Plane	Symmetry	Symmetry

Table 2 Boundary conditions for CFD and heat transfer simulations

3.2 Turbulent Flow Model

In fluid mechanics, the Reynolds number characterizes the flow regime. The flow can be laminar or turbulence, depending on the value of Re. High Re flows are expected to be turbulent while low Re flows are laminar. The Reynolds number for this flow is calculated as

$$Re = \frac{VD_H}{\nu} \tag{1}$$

where D_H = 50mm is the hydraulic diameter, V is the average velocity and ν is the kinematic viscosity of the fluid.

In the present work, the flow and heat transfer characteristics are investigated for four different values of Re as listed in Table 3. The flow in the tube zone is turbulent for all four value of Re selected. The flow structure predicted for Re = 1500 and 400 are compared against that observed by Yayla [32].

Average speed (V)	***Re***
0.014 m/s	700
0.03m/s	1,500
0.08m/s	4,000
0.12 m/s	6,000

Table 3Thelist of Reynolds number simulations conducted at various flow rates

Even though the flow inside the channel for Re = 700 and 1500 is laminar, the flow in the tube bundle region is turbulent. To illustrate that, the laminar model is used to perform the simulation for Re = 700 with "Finer" mesh. The calculated residual of continuity did not converge as shown in Figure7.The residual of continuity and x-component for a laminar model (A) and a turbulent model (B) is displayed here. The turbulent model yields a converged solution while a laminar model does not as the number of iteration is increased.

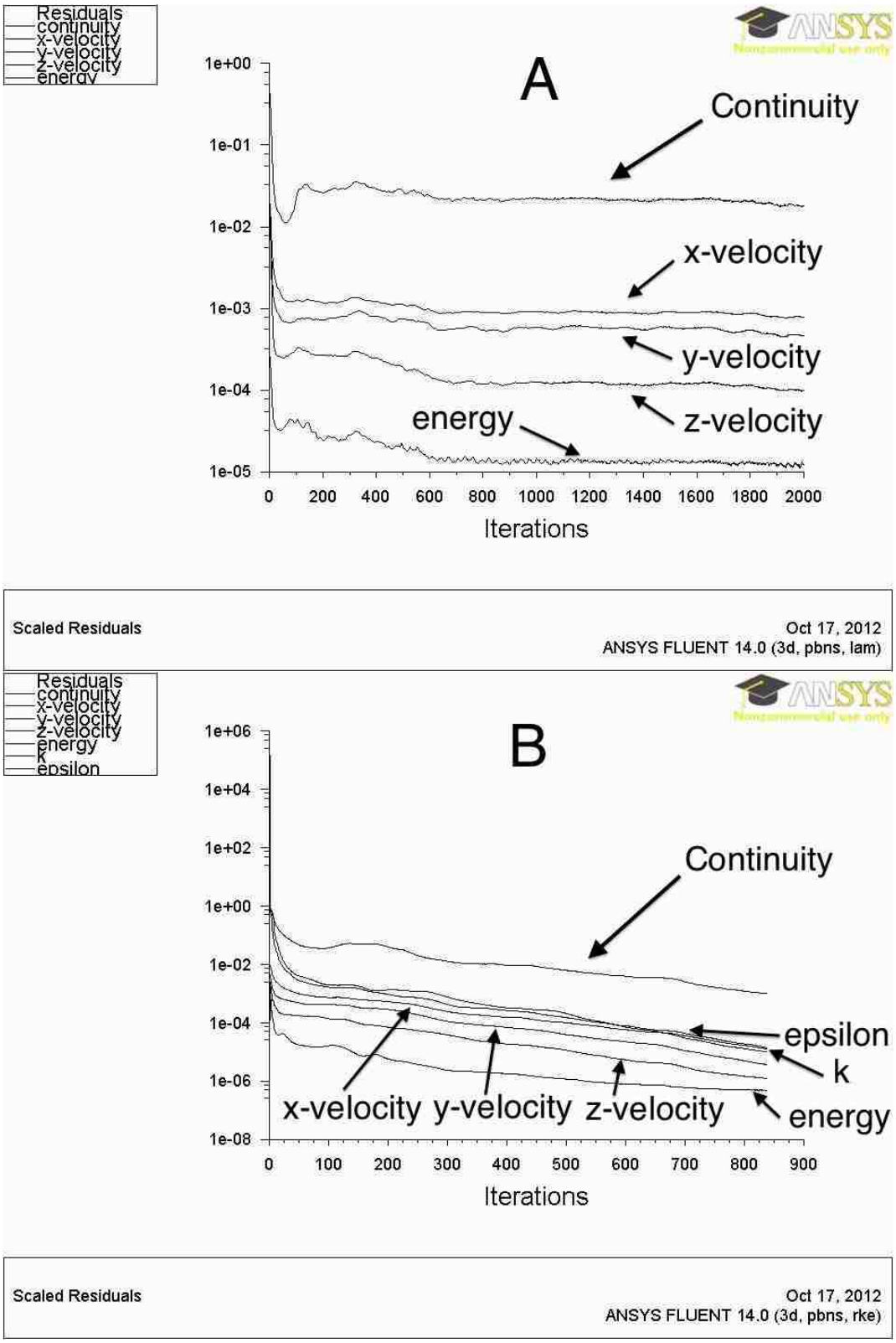

Figure 7 Residuals in various flow parameters for Re = 700 for a laminar and turbulent flow modeling

Turbulent flows are characterized by fluctuating velocity and pressure fields. In practice, the turbulent flows contain small scale eddies having high frequency fluctuations. It will be very computationally intensive to solve the Navier-Stokes equation directly to determine such flow structures. To make the numerical simulation to be feasible, the governing equations can be modified and additional variables are introduced by using a time averaging scheme. Small-scale fluctuations can be filtered. Reynolds-Averaged-Navier-Stokes (RANS), was introduced by researchers as an alternative. The RANS model, which decomposes instantaneous quantity into time-averaged and fluctuated quantities, is the most widely used model for industrial flows. By applying the decomposition to all the quantities, the instantaneous continuity and momentum equations yield the ensemble-averaged equations as:

$$\frac{\partial \rho}{\partial t} + \frac{\partial}{\partial t}(\rho u_i) = 0 \tag{2}$$

$$\frac{\partial}{\partial x_j}(\rho u_i u_j) + \frac{\partial}{\partial t}(\rho u_i) = -\frac{\partial p}{\partial x_i} + \frac{\partial}{\partial x_j}\left[\mu\left(\frac{\partial u_i}{\partial x_j} + \frac{\partial u_j}{\partial x_i} - \frac{2}{3}\delta_{ij}\frac{\partial u_l}{\partial x_l}\right)\right] + \frac{\partial}{\partial x_j}\left(-\rho\overline{u_i{}' u_j{}'}\right) \tag{3}$$

where u_i is the time averaged velocity vector, ρ is the density, μ is the viscosity of the fluid, δ_{ij} is the Kronecker delta ($\delta_{ij} = 0$ for i ≠ j and $\delta_{ij} = 1$ for i = j), t is the time and x_i is the spatial coordinated.

Equations [2, 3] are so called RANS equations which represent the same form as the instantaneous Navier-Stokes equation with the time-averaged values for the velocity and the pressure. In equation (3), $\left(-\rho\overline{u_i{}' u_j{}'}\right)$represents the Reynolds stresses, which must be modeled in order to close equation (3).

ANSYS FLUENT provided several RANS turbulence models, such as Spalart-Allmaras One-Equation Model, k-ε model, k-ω model and Reynolds Stress Model (RSM). The k-ε model is selected for the simulation and more detailed discussions are presented in the next section.

3.3 k-ε RANS Model

The two-equation realizable k-ε model, proposed by Shih et al[34], is employed to model the turbulent flow. Besides the typical continuity and momentum equations, the realizable k-ε model modified the traditional k-ε model by introducing a new eddy-viscosity formula with a variable C_μ and a new model equation for dissipation (ε). The transport equations for this model are presented as:

$$\frac{\partial}{\partial t}(\rho k) + \frac{\partial}{\partial x_j}(\rho k u_j) = \frac{\partial}{\partial x_j}\left[\left(\mu + \frac{\mu_t}{\sigma_k}\right)\frac{\partial k}{\partial x_j}\right] + G_k + G_b - \rho\varepsilon - Y_M + S_k \tag{4}$$

whereG_k is the generation of turbulence kinetic energy due to the mean velocity gradients:

$$G_k = -\rho\overline{u_\iota u_J}\frac{\partial u_j}{\partial x_i} \tag{5}$$

$G_b$is the generation of turbulence kinetic energy due to buoyancy, and Y_M represents the contribution of the fluctuating dilatation in compressible turbulence to the overall dissipation rate.

$$\frac{\partial}{\partial t}(\rho\varepsilon) + \frac{\partial}{\partial x_j}(\rho\varepsilon u_j) = \frac{\partial}{\partial x_j}\left[\left(\mu + \frac{\mu_i}{\sigma_\varepsilon}\right)\right] + \rho C_1 S\varepsilon - \rho C_2 \frac{\varepsilon^2}{k+\sqrt{\nu\varepsilon}} + C_{1\varepsilon}\frac{\varepsilon}{k}C_{3\varepsilon}G_b + S_\varepsilon \tag{6}$$

where,

$$C_1 = max\left[0.43, \frac{\eta}{\eta+5}\right] \qquad C_{3\varepsilon} = \tanh\left|\frac{v}{u}\right|$$

where,

$$\eta = S\frac{k}{\varepsilon}S = \sqrt{2S_{ij}S_{ij}}$$

The eddy viscosity is computed from

$$\mu_t = \rho C_\mu \frac{k^2}{\varepsilon} \tag{7}$$

The C_μ in the realizable k-ε model is a variable and calculated by

$$C_\mu = \frac{1}{A_0 + A_s\frac{kU^*}{\varepsilon}} \tag{8}$$

where

$$U^* = \sqrt{S_{ij}S_{ij} + \widetilde{\Omega}_{ij}\widetilde{\Omega}_{ij}} \tag{9}$$

and

$$\widetilde{\Omega}_{ij} = \Omega_{ij} - 2\varepsilon_{ijk}\omega_k \tag{10}$$

$$\Omega_{ij} = \overline{\Omega}_{ij} - \varepsilon_{ijk}\omega_k \tag{11}$$

where Ω_{ij} is the mean rate-of-rotation tensor viewed in a moving reference frame.

$$A_0 = 4.04, \quad A_s = \sqrt{6}\cos\phi \tag{12}$$

where

$$\phi = \frac{1}{3}\cos^{-1}\left(\sqrt{6}W\right), \quad W = \frac{S_{ij}S_{jk}S_{ki}}{\tilde{S}^3}, \quad \tilde{S} = \sqrt{S_{ij}S_{ij}}, \quad S_{ij} = \frac{1}{2}\left(\frac{\partial u_j}{\partial x_i} + \frac{\partial u_i}{\partial x_j}\right) \tag{13}$$

The values for other parameters are:

$$C_{1\varepsilon} = 1.44, \quad C_2 = 1.9, \qquad \sigma_k = 1.0, \qquad \sigma_\varepsilon = 1.2$$

and S_ε , S_k are additional source terms for k and ε.

3.4 Heat Transfer Model

Being strongly linked to the turbulence model, the heat transfer simulation, for eddy viscosity models, is generally based on the analogy between the heat and the momentum transfer. In FLUENT, the turbulent heat transport is modeled using the concept of Reynolds' analogy to turbulent momentum heat transfer. The energy equations are coupled and solved simultaneously, with introduction of constant turbulent Prandtl number. Turbulent energy equation is given by,

$$\frac{\partial}{\partial t}(\rho E) + \frac{\partial}{\partial \mathrm{x}_i}[u_i(\rho E + p)] = \frac{\partial}{\partial \mathrm{x}_j}\left(k_{eff}\frac{\partial T}{\partial x_j} + u_i\left(\tau_{ij}\right)_{eff}\right) + S_h \tag{13}$$

where E is the total energy, calculated by,

$$E = h - \frac{p}{\rho} + \frac{v^2}{2} \tag{14}$$

for incompressible flows,

$$h = \sum_j Y_j h_j + \frac{p}{\rho} h_j = \int_{T_{ref}}^{T} c_{p,j} dT \qquad (T_{ref}\text{=298.15K}) \tag{15}$$

And k_{eff} is the effective thermal conductivity,

$$k_{eff} = k + \frac{c_p \mu_t}{Pr_t} \tag{16}$$

Hence, k is the thermal conductivity and the default value for turbulent Prandtl number Pr_t = 0.85.

$(\tau_{ij})_{eff}$ is the deviatoric stress tensor and it is defined as

$$(\tau_{ij})_{eff} = \mu_{eff}\left(\frac{\partial u_j}{\partial x_i} + \frac{\partial u_i}{\partial x_j}\right) - \frac{2}{3}\mu_{eff}\frac{\partial u_k}{\partial x_k}\delta_{ij} \quad (17)$$

Item involving $(\tau_{ij})_{eff}$ represents the viscous heating and it is not computed by default in pressure-based solver.

3.5 Solution Procedure

Hybrid initialization method is applied for initializing the velocity and temperature fields in the computational domain. The velocity filed and pressure field are generated by solving the Laplace equation. Temperature field and the turbulent parameters are initialized with domain-averaged values. Together with the continuity and momentum equations, the two equations of k-ε model will be solved with the SIMPLE algorithm. In order to achieve better accuracy, the second-order discretization is applied to the tetrahedral and hexahedral meshes in the computational domain.

Chapter 4. Results Discussion

Particle Image Velocimetry (PIV) flow visualizations illustrate that the turbulent intensity increases as the flow passed through each row of slotted tubes. The increased turbulent intensity helps improving the rate of heat transfer in the heat exchanger. Flow structures in the tube zone observed and predicted are compared in this chapter. The effect of slotted tube on the heat transfer performance is investigated by comparing the heat transfer from slotted tubes against that from traditional non-slotted tubes.

4.1 Flow Characteristics

3D flow structure is investigated near wall and away from the boundary for the Reynolds number of 1500. The streamlines, vorticity, stream-wise and span-wise components of the velocity vector and turbulent kinetic energy coefficient contours are examined at various planes. Figure8 displays these contours at z = 0.05 h, 0.4h and 0.5h (at the centerline) for Re =1500.

Flow separates near π/2 at z = 0.4h & 0.5h while it separates further downstream near the wall indicated by the streamlines shown in Figure8. In the wall region vortices near the slit and around the tube are not as intense as the vortices near the centerline, as shown in Figure9. The effect of the wall on the flow structure is obvious, but it is not profound, as shown in the velocity and vorticity fields at z = 0.05h for Re =1500.

2D counterpart of the flow is simulated in x-y plane for Re =1500. The contours of streamline, vorticity, stream-wise and span-wise components of the velocity vector and the turbulent kinetic energy coefficient are plotted in Figure10 for Re =1500 and Figure11 *for* Re =4000. 2-D flow structure is directly compared against the 3-D flow

structure at the centerline. Even though velocity and vorticity field are very similar qualitatively, the shape, distribution and the magnitude of the vortices are different. This proved that it is important to employ 3-D flow modeling to capture the flow field in the tube bank region of the heat exchanger.

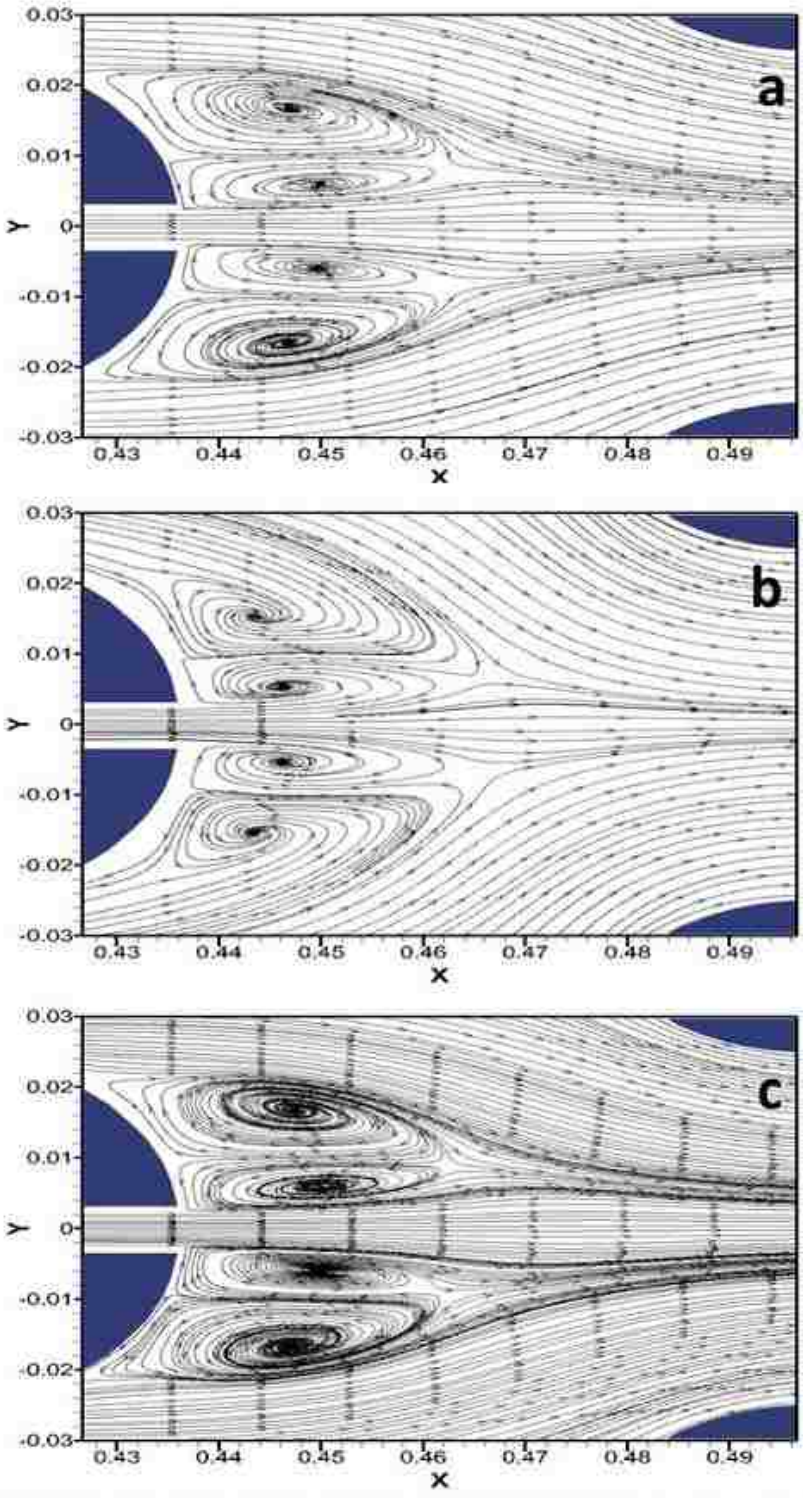

Figure 8 Stream function for Re =1500 at various cross-sections: (a) z = 8 mm; (b) z = 1 mm; (c) z = 10 mm

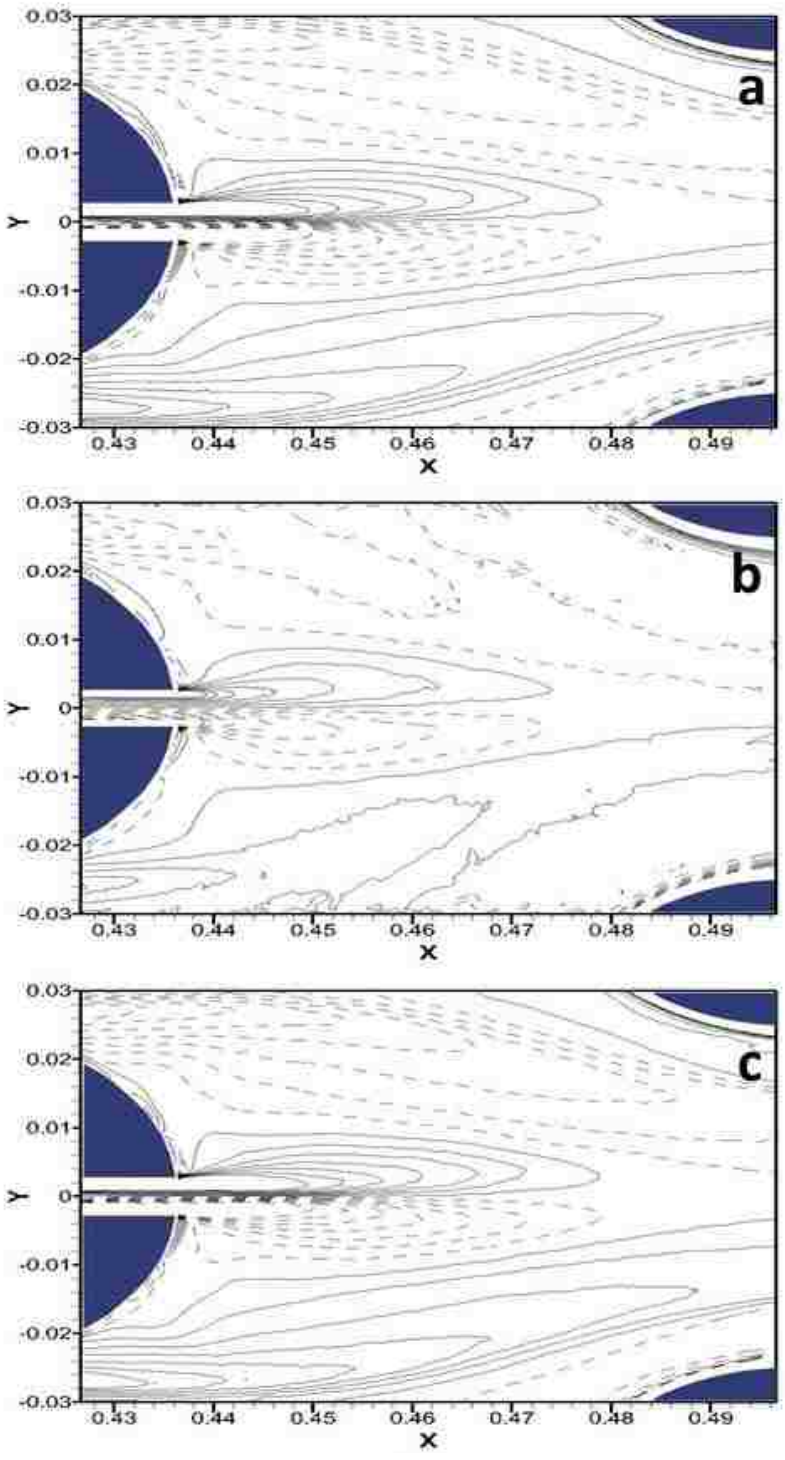

Figure 9 Vorticity Contours for Re = 1500 at various cross-sections: (a) z = 8 mm; (b) z = 1 mm; (c) z = 10 mm

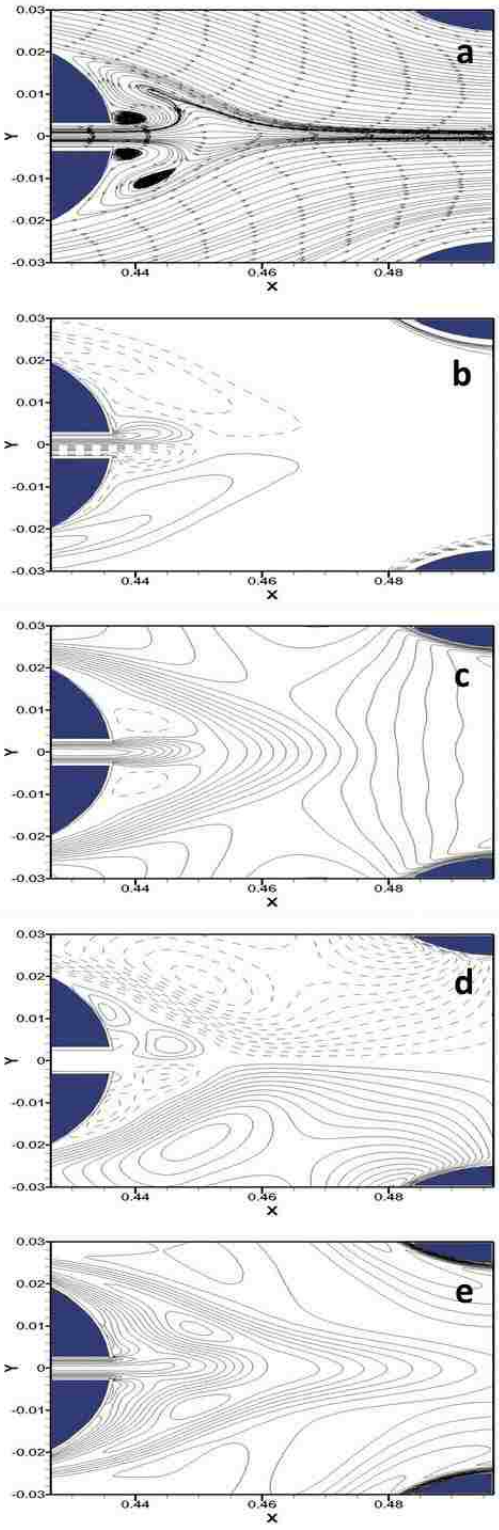

Figure 10 (a) Streamline; (b) Vorticity; (c) Stream-wise velocity; (d) Span-wise velocity; (e) Turbulent kinetic energy contours predicted by 2-D model for Re =1500

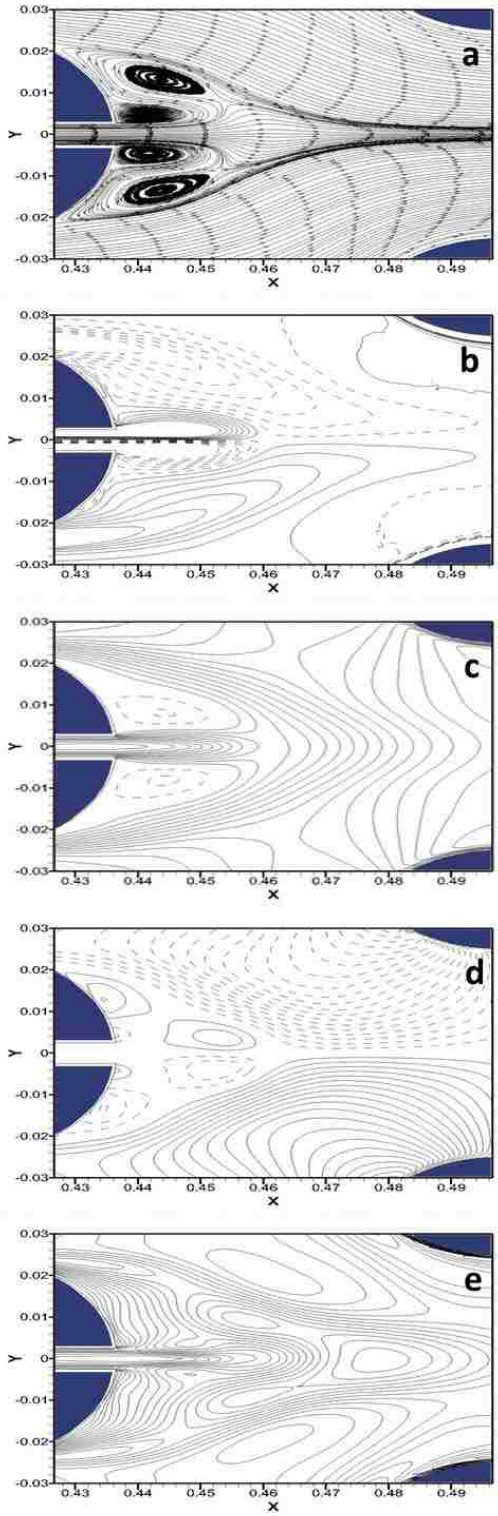

Figure 11 (a) Streamline; (b) Vorticity; (c) Stream-wise velocity; (d) Span-wise velocity; (e) Turbulent kinetic energy contours predicted by 2-D model for Re = 4000

4.2 Comparison between Simulations & Experiments

Images of the flow field is acquired at the X-Y plane in the middle of the channel at z = 10 mm (0.5h). The streamlines, vorticity, stream-wise and span-wise components of the velocity vector and the turbulent kinetic energy coefficient are experimental determined by averaging 350 PIV images [32]. Numerical simulations for the velocity and temperature fields are conducted using ANSYS FLUENT and graphical forms of results are presented using TECPLOT software. The streamline patterns, vorticity contour, time-averaged velocity components and turbulent kinetic energy (TKE) predicted and observed are compared for Re = 1500 and 4000.

Streamline patterns predicted by 2D & 3D computational fluid dynamic simulations and obtained by the PIV flow visualizations for Reynolds number of 1500 are illustrated in Figure12. Flow is separated at downstream of the slotted tube. The separation predicted by 2D simulation occurs nearly 45^o degrees while 3-D simulation predicts that the separation occurs nearly 90^odegree angle, as shown in Figure12a and 12b. The streamlines are symmetric about the axis of the tube, they are detached at the downstream of the tube and are attached again about the midpoint between two arrays. There are two pairs of counter rotating vortices. The pair of vortices near the tube axis predicted by 2-D simulation is much smaller than that predicted by 3-D model. The pattern of the streamline predicted by 3-D model agrees very well with that observed by the experiments, as shown in Figure12. The similar flow characteristics are obtained for Re= 4000. 3-D model predicts the flow patterns much better than 2D model. The presence of walls at the bottom and top of the channel has an influence on the flow field not only near the wall region, but everywhere.

Figures14and 15display the vorticity contours predicted by 2D & 3D models and observed by the experiments for Reynolds number of 1500 and 4000.The minimum level of vorticity for both values of Re is $\pm 1 s^{-1}$with increment value of $2 s^{-1}$. A pair of counter rotating vortices is formed near the rear stagnation point of the tube around the outlet of the slot and extends downstream. Another pair of counter rotating vortices is formed at an angel about$\pi/2$ at each side of the tube. The spatial structure of vortices predicted by 2D model agree qualitatively with those observed by the experiment. Vorticity field predicted by the 3D model agree much better with the observed vorticity field for both Re = 1500 and 4000, as shown in Figures 14 and 15.

Figure 16 displayed the normalized stream-wise component of the velocity (<u>/U) and the normalized span-wise component of the velocity vector (<v>/U) and the turbulent kinetic energy predicted and observed for the Reynolds number of 4000.The minimum value for the normalized stream-wise velocity (<u>/U) is 0.025 with an increment Δ[<u>/U] =0.025. For the normalized span-wise velocity (<v>/U), the minimum value is $(<v>/U)_{min}$ = 0.05 and the increment value is Δ[<u>/U] =0.05. The velocity predicted by 3D model and observed by the experiments match well, as shown in Figure 16. This is another illustration that 3D model captures the flow field observed by the experiments documented by Yayla [32].

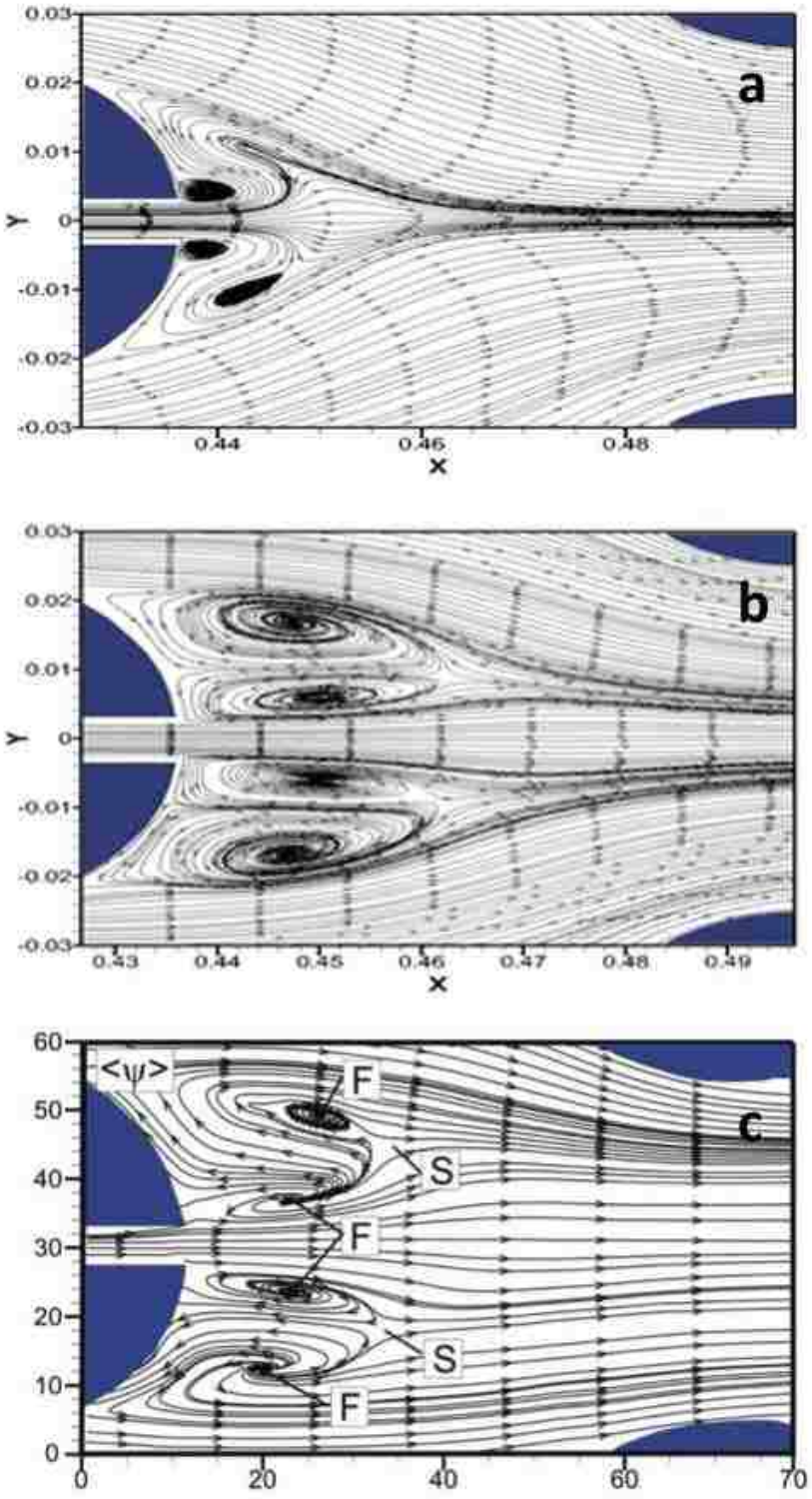

Figure 12 Stream function for Re =1500 predicted by (a) 2D simulation, (b) 3D simulation and (c) observed by experiments

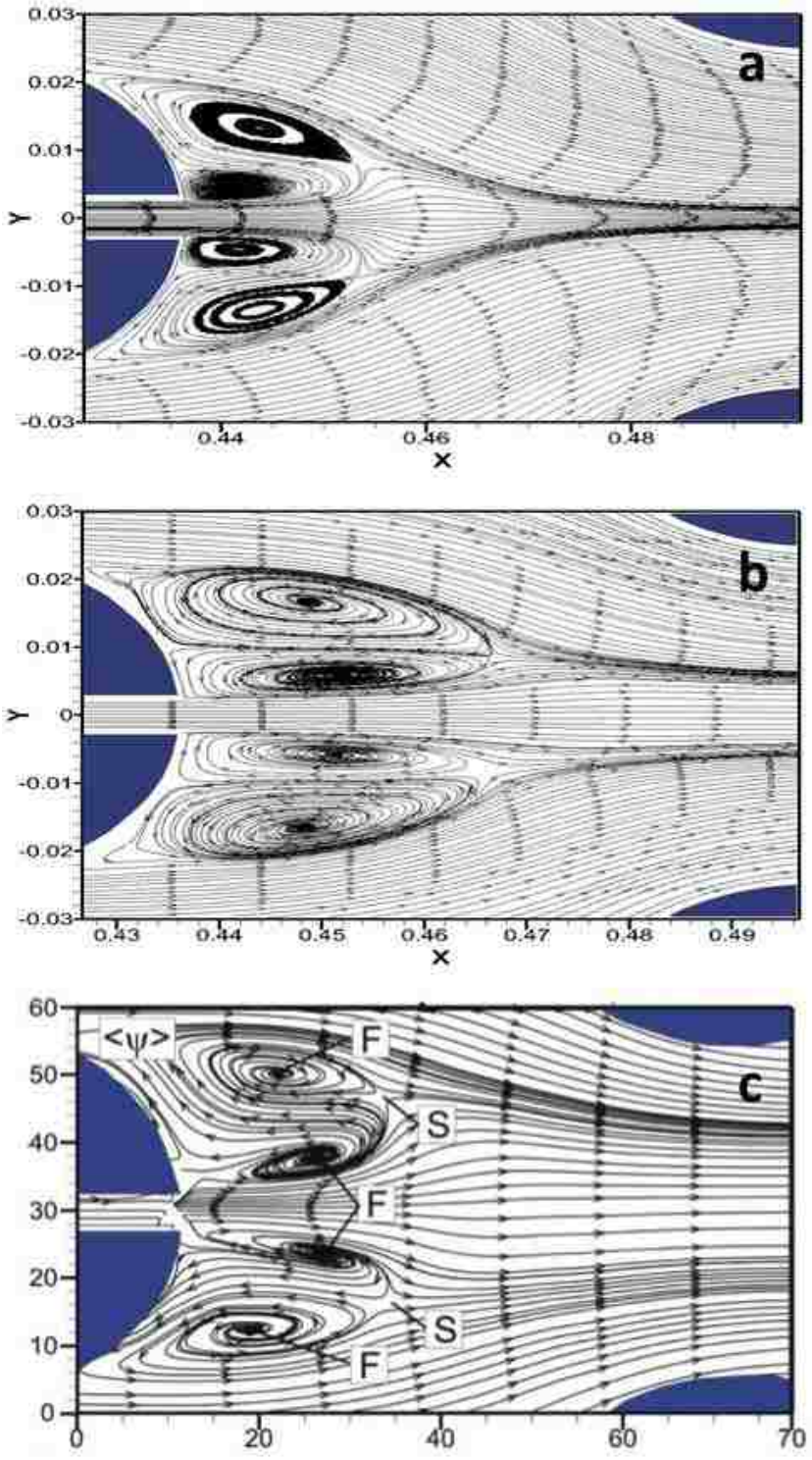

Figure 13 Stream function for Re = 4000 predicted by (a) 2D simulation, (b) 3D simulation and (c) observed by experiments

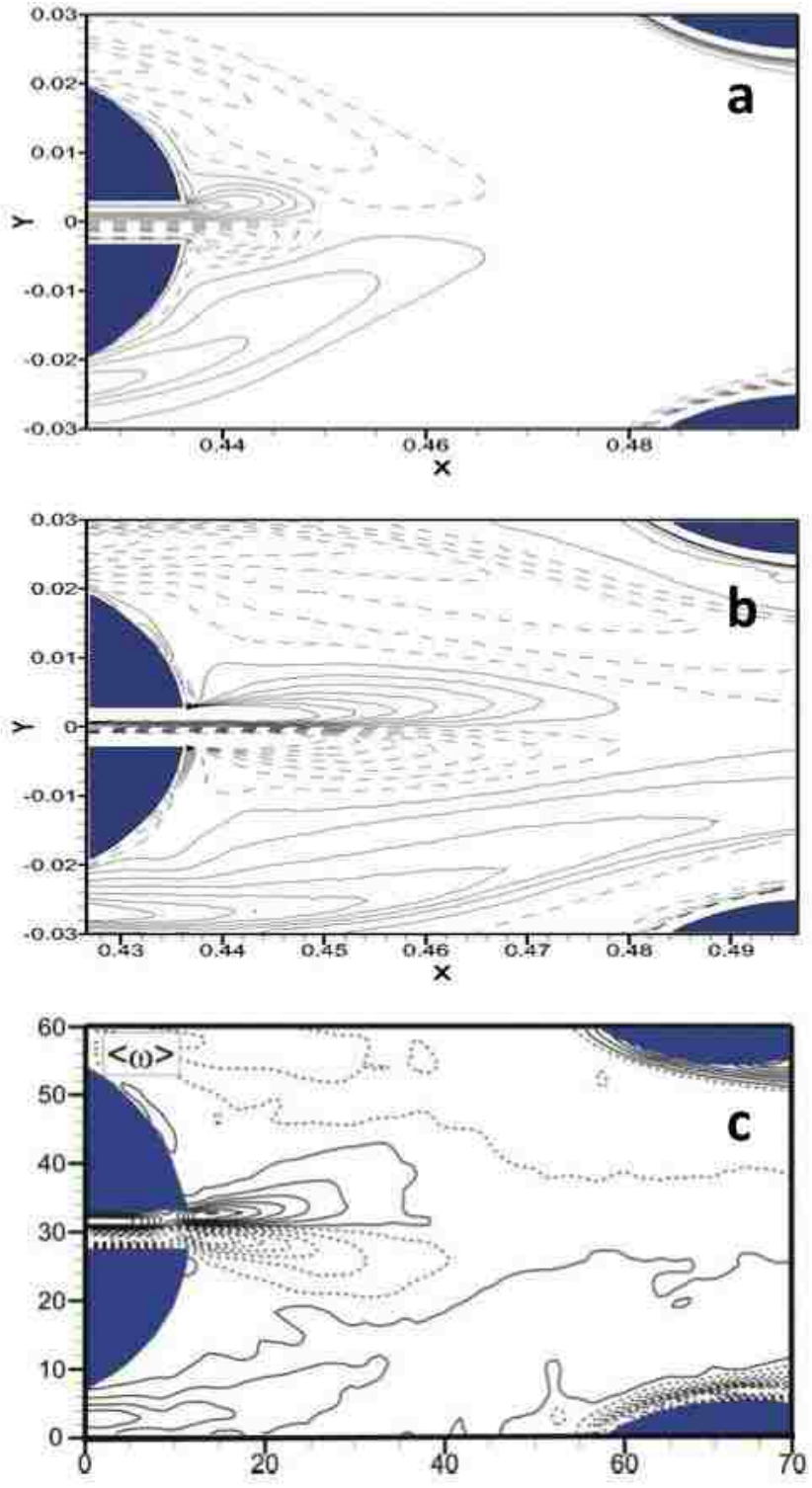

Figure 14 Vorticity contours for Re = 1500 predicted by (a) 2D simulation, (b) 3D simulation and (c) observed by experiments. Minimum value of vorticity is ±1s-1 and the increments is $\Delta\omega$=2s-1

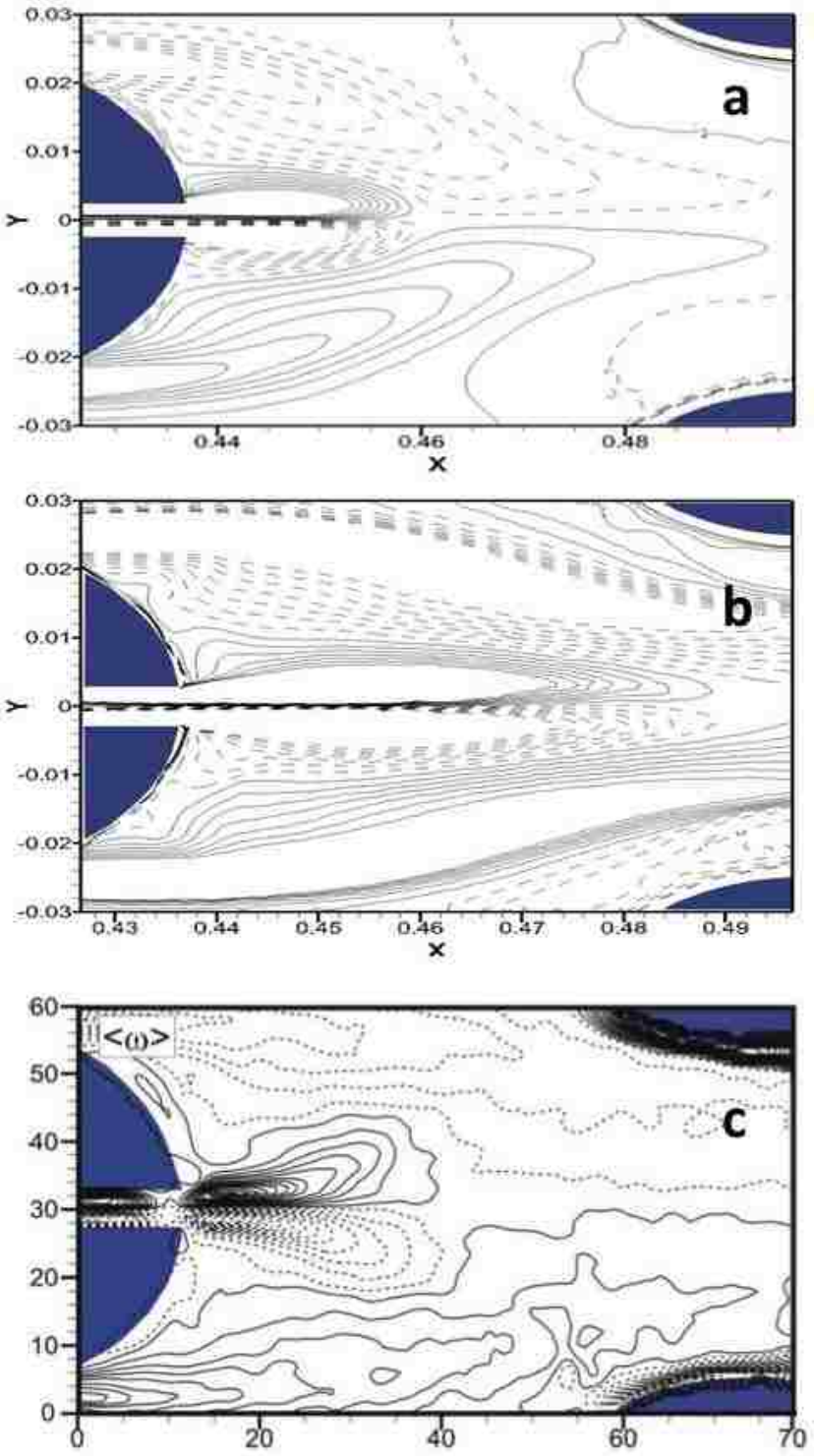

Figure 15 Vorticity contours for Re = 4000 predicted by (a) 2D simulation, (b) 3D simulation and (c) observed by experiments. Minimum value of vorticity is ±1s-1 and the increments is Δω=2s-1

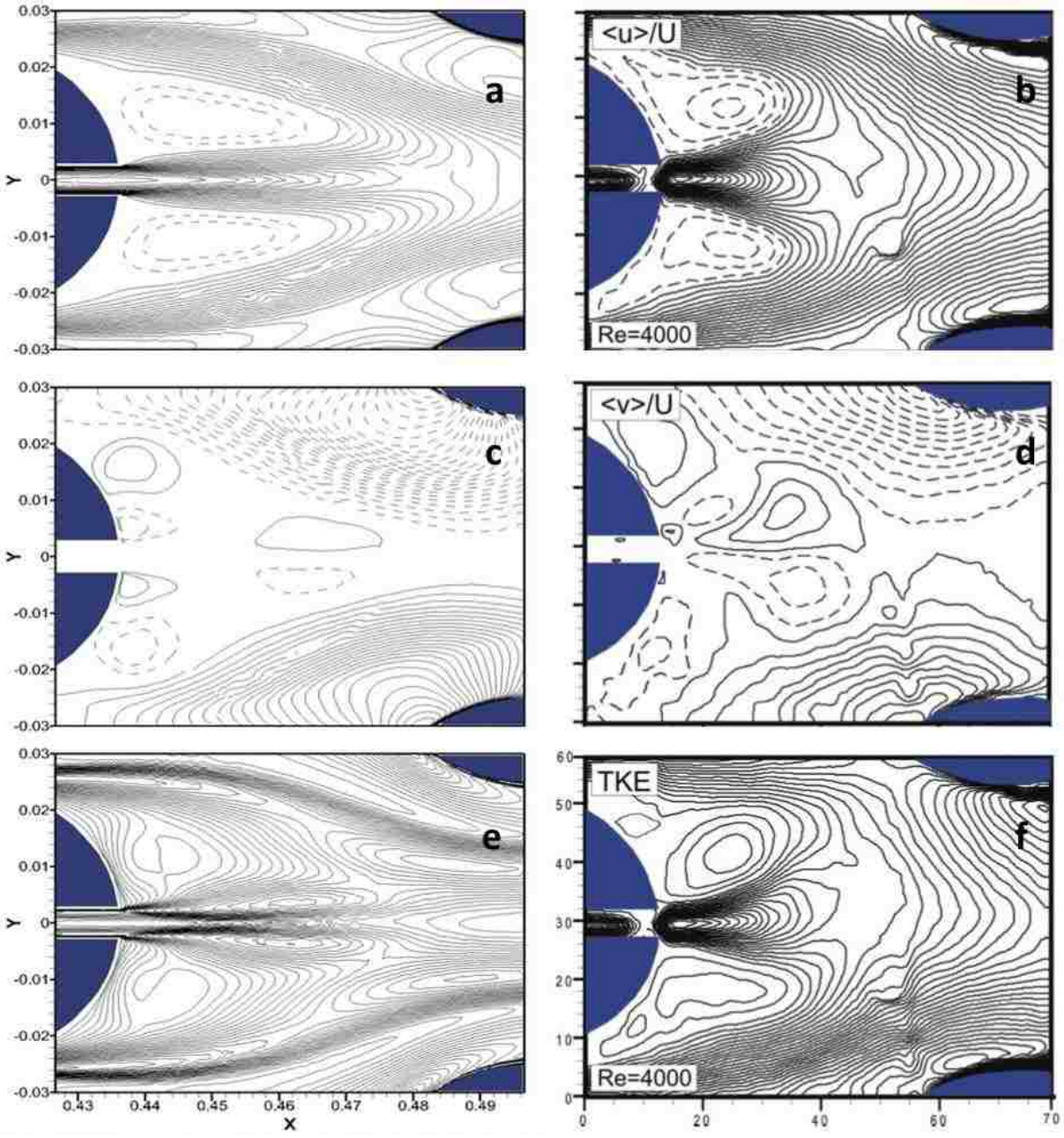

Figure 16 Normalized stream-wise velocity [<u>/U], span-wise velocity [<v>/U] and turbulent kinetic energy for Re =4000. Contours at the left column denote results predicted by 3D simulations; contours at the right column denote results obtained by experimental measurements. Minimum of [<u>/U] is 0.025and the minimum of [<v>/U] is 0.05 with the increments of Δ[<u>/U] is 0.025 and the increments of Δ[<v>/U] is 0.05

4.3 Heat Transfer Analysis

Convective heat transfer simulation is conducted for the tube bank heat exchanger without slots to validate the numerical methods and to evaluate the effect of the slotted tube on the performance of the heat exchanger. Empirical heat transfer correlations for flow passing staggered tube bank is presented in a tabular form in Incropera et al. [30].

$$\overline{\mathrm{N}_u} = 1.13 C_1 {Re_{D,max}}^m (Pr)^{1/3} \tag{18}$$

For,

S_T = 2D=100mm, S_D = 2D=100mm, S_L = D=86.603mm, D = D_H=50mmm,

$$V_{max} = \frac{S_T}{2(S_D - D)} \mathrm{V} \tag{19}$$

$$Re_{D,max} = \frac{V_{max} D_H}{\nu} = 1500 \tag{20}$$

According to the tabular data, C_1 = 0.467, m=0.562.The Prandtl number, Pr for water is 7. The averaged value of N_u is determined to be

$$\overline{\mathrm{N}_u} = \frac{\bar{h} D_h}{k} = 1.13 * 0.467 {Re_{D,max}}^{0.562} (7)^{\frac{1}{3}} = 61.53 \tag{21}$$

Using the definition of N_u, the average value of the heat transfer coefficient is

$$\bar{h} = \frac{\overline{\mathrm{N}_u} k}{D_H} = 615.3\ W/m^2K \tag{22}$$

The convective heat transfer simulation for the non-slot tube bank for Re = 700, 1500, 4000 and 6000 is conducted. The Heat transfer coefficient is determined along the surface of the tube. By investigating the local value of the heat transfer coefficient along the surface of the tube, the total heat transfer coefficient is determined for Re = 1500 as

$$h_{Total} = 48.21(W/m^2K)(m^2) \quad (23)$$

The averaged value of heat transfer coefficient is calculated as

$$\bar{h} = \frac{h_{Total}}{Total\ Tube\ Surface\ Area} = \frac{48.21}{0.0785} = 614.1 W/m^2K \quad (24)$$

	Empirical Correlation	Numerical Simulation	Error
$\bar{h}\ (W/m^2K)$	615.3	614.1	0.2%

Table 4 Averaged heat transfer coefficient for non-slot design

Predicted value of the heat transfer coefficient agrees with the tabulated value within 0.2% accuracy, as displayed in Table 4. This validates the 3D convective heat transfer simulations conducted in the present work. The isotherms for the non-slot and the slotted arrays of tube are shown in Figures 17 and 18. Figures 17displays isotherms in the wake of non-slotted and slotted tube for Re = 1500. It is clear from the temperature field that the presence of the slot in the stream-wise direction enhances the heat transfer between the fluids and the arrays of the tube. The one slowly rotating vortex pair is present near the rear stagnation point of the non-slotted tube, as shown in Figure 17 c-f. On the other hand, another pair of vortex near the exit of the slot at the back of tube is formed and the vortex near the top and bottom of the cylinder extend further downstream. That increases the heat transfer from the tube to the fluid, also indicated by the comparison of isotherms as shown in Figures 17 and 18.

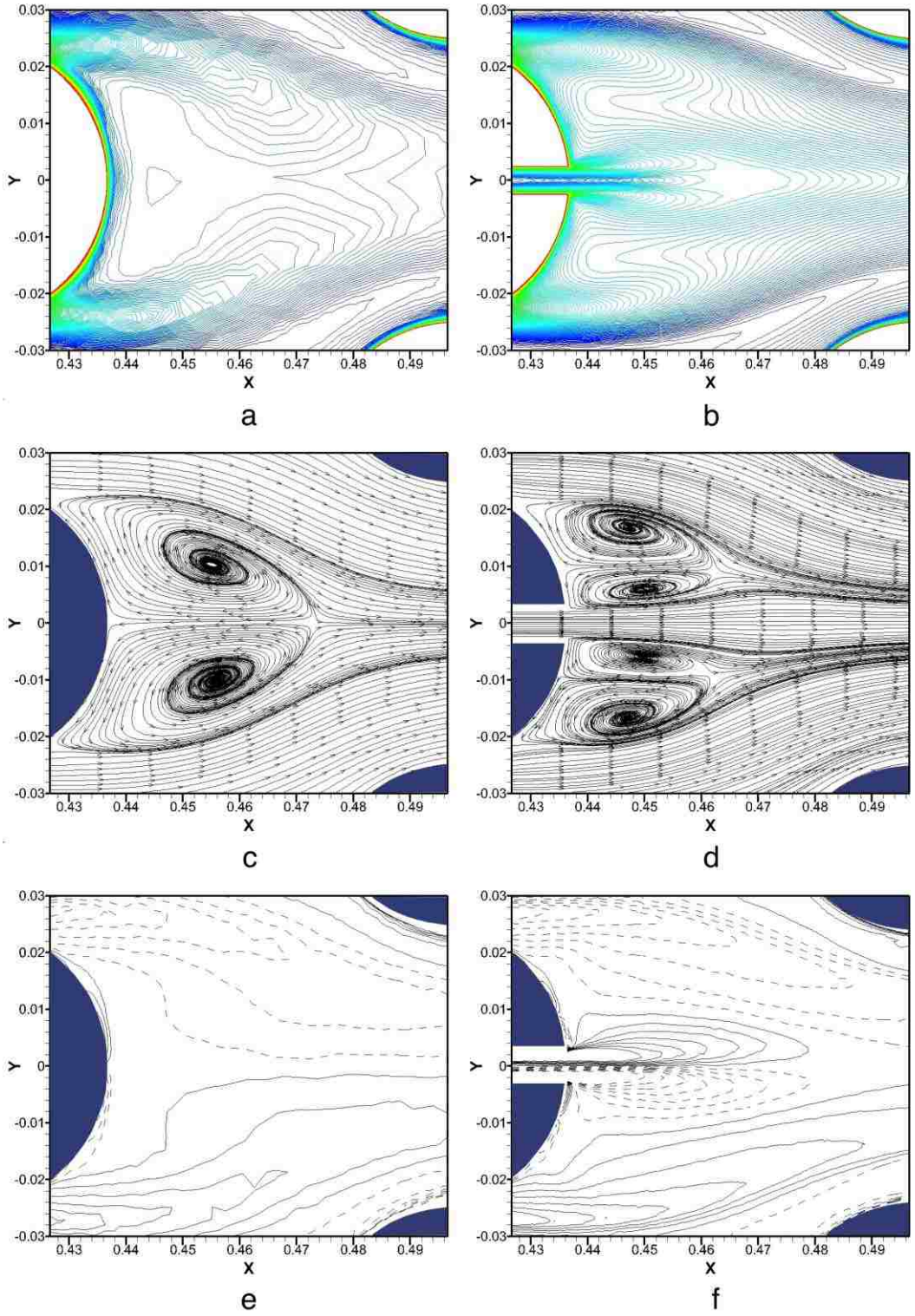

Figure 17 Isotherms (first row- a, b), streamlines (the second row- c, d) and vorticity field(third row- e, f) for Re =1500 in the wake a tube. Contours at the left column denote results obtained for the non-slotted tube design and the contours at the right denote results for the slotted tube design

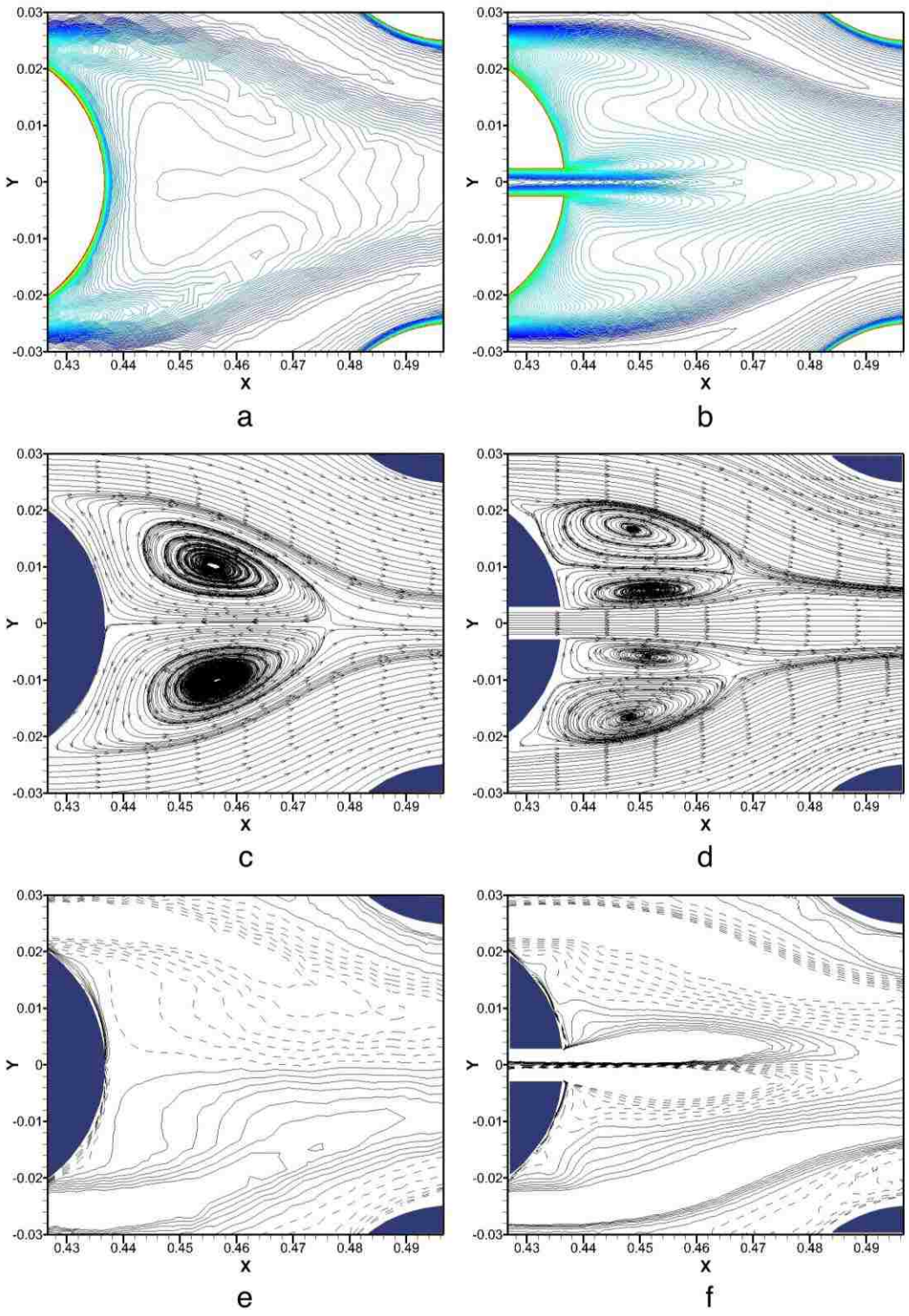

Figure 18 Isotherms (first row- a, b), streamlines (the second row- c, d) and vorticity field (third row- e, f) for Re = 4000 in the wake a tube. Contours at the left column denote results obtained for the non-slotted tube design and the contours at the right denote results for the slotted tube design

The cooler fluid flow from left to right as it passes the array of tubes. It is heated by the tubes. The thermal energy was exchanged and contours of isotherms match with the patterns of the velocity. It is noted that the fluid temperature at the exit of tube bundle is higher than that for the un-slotted bundles. That shows that the performance of the slotted tube heat exchanger is significantly better than that of the non-slotted tube heat exchanger.

For Re = 1500, the total surface heat transfer coefficient obtained from the simulation for slotted design is

$$h_{Total} = 90.87(W/m^2K)(m^2)$$

The averaged heat transfer coefficient is

$$\bar{h} = \frac{h_{Total}}{Total\ Tube\ Surface\ Area} = \frac{90.87}{0.117} = 776.7\ W/m^2K$$

The averaged heat transfer coefficient of the slotted tube heat exchanger is 27% greater than the heat transfer coefficient of the traditional tube heat exchangers. The averaged heat transfer coefficient predicted for the slotted tube bundle heat exchanger is determined from the 3D convective heat transfer simulations for Re =700,1500,4000 and 6000. The averaged heat transfer coefficient for the same values of Re is also determined from empirical correlations as described below. Heat exchanger with the slotted tube bundle heat exchangers perform much better for all Re considered in the present work.

Re	Non-slotted	Slotted	Improvement
700	400.9	499.3	25%
1500	614.1	776.7	27%
4000	1067.7	1625.6	53%
6000	1341.0	2054.9	53%

Table 5 Comparison of heat transfer performance between slotted and non-slotted heat exchanger designs for Re = 700, 1500, 4000 and 6000

Chapter 5.Conclusion

3D turbulent flow structure and the heat transfer performance of the novel shell-tube heat exchanger have been investigated. The turbulent flow characteristic in the tube region is modeled by k-ε Reynolds stress averaging model. 3-D unsteady flow and heat transfer simulations are performed for Reynolds number 700, 1500, 4000 and6000. Spatial flow characteristic predicted by computational fluid dynamic simulations agree very well with those observed by the Particle Image Velocimetry experiments conducted by Yayla [32] for Re = 1500 and 4000. Comparison between 3D and 2D flow simulations reveals that the spatial structure of vortices formed in the wake of slotted tube is influenced by the presence of wall. That could have profound effects on the performance of the shell-tube heat exchanger.

Heat transfer performance of the slotted tube heat exchangers are determined and compared against that of traditional non-slotted tube heat exchangers. It has been shown that small slots in the stream-wise direction enhance the performance of the heat exchangers as much as 53%. Slotted heat exchanger has 25 to 53% higher heat transfer rate compared to the non-slotted tube heat exchanger for Reynolds number from 700 to 6000. It is also shown that the improvement in the heat transfer rate increases at higher flow rates. Even though the manufacturing expense for the semicircle tubes is much higher, the slotted design might still be feasible. The slotted tube bank heat exchanger is believed to have broad industrial applications.

The significance of the slot on heat transfer has been examined by the present study. The width of the slot width and its direction can have strong influence on the heat transfer

performance of the slotted shell tube heat exchanger. Such effects will be examined as part of the future study.

Reference

[1] Oztekin A., Neti S., and Ukaew A., 2010, "Effects of Nanoparticles and Polymer Additives in Turbulent Pipe Flow," ASME Conf. Proc., 2010(44465), pp. 761–766.

[2] Muley A., and Manglik R. M., 1999, "Experimental study of turbulent flow heat transfer and pressure drop in a plate heat exchanger with chevron plates," J. Heat Transfer, 121(1), pp. 110–117.

[3] Leu J.-S., Wu Y.-H., and Jang J.-Y., 2004, "Heat transfer and fluid flow analysis in plate-fin and tube heat exchangers with a pair of block shape vortex generators," International Journal of Heat and Mass Transfer, 47(19-20), pp. 4327–4338.

[4] Torii K., Kwak K. M., and Nishino K., 2002, "Heat transfer enhancement accompanying pressure-loss reduction with winglet-type vortex generators for fin-tube heat exchangers," International Journal of Heat and Mass Transfer, 45(18), pp. 3795–3801.

[5] Hwang S. W., Kim D. H., Min J. K., and Jeong J. H., 2012, "CFD analysis of fin tube heat exchanger with a pair of delta winglet vortex generators," J Mech Sci Technol, 26(9), pp. 2949–2958.

[6] Jang J. Y., and Chen L. K., 1997, "Numerical analysis of heat transfer and fluid flow in a three-dimensional wavy-fin and tube heat exchanger," International Journal of Heat and Mass Transfer, 40(16), pp. 3981–3990.

[7] Nuntaphan A., Kiatsiriroat T., and Wang C. C., 2005, "Air side performance at low Reynolds number of cross-flow heat exchanger using crimped spiral fins," International Communications in Heat and Mass Transfer, 32(1-2), pp. 151–165.

[8] Matos R. S., Vargas J., Laursen T. A., and Saboya F., 2001, "Optimization study and heat transfer comparison of staggered circular and elliptic tubes in forced convection," International Journal of Heat and Mass Transfer, 44(20), pp. 3953–3961.

[9] Eiamsa-ard S., and Promvonge P., 2007, "Heat transfer characteristics in a tube fitted with helical screw-tape with/without core-rod inserts," International Communications in Heat and Mass Transfer, 34(2), pp. 176–185.

[10] Eiamsa-ard S., and Promvonge P., 2010, "Performance assessment in a heat exchanger tube with alternate clockwise and counter-clockwise twisted-tape inserts," International Journal of Heat and Mass Transfer, 53(7-8), pp. 1364–1372.

[11] Zhang J.-F., He Y.-L., and Tao W.-Q., 2009, "3D numerical simulation on shell-and-tube heat exchangers with middle-overlapped helical baffles and continuous baffles – Part II: Simulation results of periodic model and comparison between continuous and noncontinuous helical baffles," International Journal of Heat and Mass Transfer, 52(23-24), pp. 5381–5389.

[12] Khan W. A., Culham J. R., and Yovanovich M. M., 2006, "Convection heat transfer from tube banks in crossflow: Analytical approach," International Journal of Heat and Mass Transfer, 49(25-26), pp. 4831–4838.

[13] Khan W. A., Culham R. J., and Yovanovich M. M., 2007, "Optimal Design of Tube Banks in Crossflow Using Entropy Generation Minimization Method,"

Journal of Thermophysics and Heat Transfer, 21(2), pp. 372–378.
[14] Ravagnani M. A. S. S., Silva A. P., Biscaia E. C., and Caballero J. A., 2009, "Optimal Design of Shell-and-Tube Heat Exchangers Using Particle Swarm Optimization," Ind. Eng. Chem. Res., 48(6), pp. 2927–2935.
[15] Unuvar A., and Kargici S., 2004, "An approach for the optimum design of heat exchangers," Int. J. Energy Res., 28(15), pp. 1379–1392.
[16] Hilbert R., Janiga G., Baron R., and Thévenin D., 2006, "Multi-objective shape optimization of a heat exchanger using parallel genetic algorithms," International Journal of Heat and Mass Transfer, 49(15-16), pp. 2567–2577.
[17] Stanescu G., Fowler A. J., and Bejan A., 1996, "The optimal spacing of cylinders in free-stream cross-flow forced convection," International Journal of Heat and Mass Transfer, 39(2), pp. 311–317.
[18] Ali Kara Y., and Güraras Ö., 2004, "A computer program for designing of shell-and-tube heat exchangers," Applied Thermal Engineering, 24(13), pp. 1797–1805.
[19] El-Shaboury A. M. F., and Ormiston S. J., 2005, "Analysis of Laminar Forced Convection of Air Crossflow in In-Line Tube Banks with NonSquare Arrangements," Numerical Heat Transfer, Part A: Applications, 48(2), pp. 99–126.
[20] Y Q Wang L A Penner S J Orm, 2000, "ANALYSIS OF LAMINAR FORCED CONVECTION OF AIR FOR CROSSFLOW IN BANKS OF STAGGERED TUBES," Numerical Heat Transfer, Part A: Applications, 38(8), pp. 819–845.
[21] Wang Y. Q., Jackson P., and Phaneuf T., 2006, "Turbulent Flow Through a Staggered Tube Bank," Journal of Thermophysics and Heat Transfer, 20(4), pp. 738–747.
[22] Uematsu Y., Tsujiguchi N., and Yamada M., 2001, "Mechanism of ovalling vibrations of cylindrical shells in cross flow," WIND STRUCT INT J.
[23] Sweeney C., and Meskell C., 2003, "Fast numerical simulation of vortex shedding in tube arrays using a discrete vortex method," Journal of Fluids and Structures, 18(5), pp. 501–512.
[24] Berger E., and Wille R., 1972, "Periodic flow phenomena," Annual Review of Fluid Mechanics.
[25] Williamson C., 1996, "Vortex dynamics in the cylinder wake," Annual Review of Fluid Mechanics, 28(1), pp. 477–539.
[26] Konstantinidis E., Balabani S., and Yianneskis M., 2003, "Relationship between vortex shedding lock-on and heat transfer: Implications for tube bundles in cross-flow," Chemical Engineering Research and Design, 81(6), pp. 695–699.
[27] Colburn A. P., 1933, A method of correlating forced convection heat transfer data and a comparison with fluid friction, American Institute of Chemical Engineers.
[28] Žukauskas A., 1972, "Heat Transfer from Tubes in Crossflow," 8, pp. 93–160.
[29] Žukauskas A., and Ulinskas R., 1988, Heat transfer in tube banks in crossflow, Hemisphere Pub. Corp., New York.
[30] Incropera F. P., and DeWitt D. P., 2001, Fundamentals of Heat and Mass Transfer, 5th Edition, Wiley.
[31] Popiel C. O., Robinson D. I., and Turner J. T., 1993, "Vortex shedding from a

circular cylinder with a slit and concave rear surface," Applied Scientific Research, 51(1), pp. 209–215.

[32] Yayla S., Beyin S., and Oztekin A., 2012, "Flow and Heat Transfer Characteristics of the Staggered Slotted Semi Cylinders in a Cross Flow Heat Exchangers," Bulletin of the American Physical Society, Volume 57, Number 17.

[33] Fox R. W., Pritchard P. J., and McDonald A. T., 2008, Introduction to Fluid Mechanics, Wiley.

[34] Shih T. H., Liou W. W., Shabbir A., Yang Z., and Zhu J., 1995, "A new k-ϵ eddy viscosity model for high reynolds number turbulent flows," Computers and Fluids, 24(3), pp. 227–238.

Vita

Haolin Ma was born in Weifang, Shandong, China, on 21 June 1986, the son of Jianwei Ma and Dongying Ma. He completed his Bachelor degree in Shandong University of Technology majoring in Mechanical Engineering in 2009. Afterwards he entered The P.C. Rossin College of Engineering and Applied Science at Lehigh University, USA, to pursue his Master of Science degree. He also participated in the Lehigh University's Industrial Assessment Center program.